High-Resolution Satellite Imagery for Mesoscale Meteorological Studies

David B. Johnson,*
Pierre Flament,+ and
Robert L. Bernstein**

Abstract

In this article high-resolution satellite imagery from a variety of meteorological and environmental satellites is compared. Digital datasets from Geostationary Operational Environmental Satellite (GOES), National Oceanic and Atmospheric Administration (NOAA), Defense Meteorological Satellite Program (DMSP), Landsat, and Satellite Pour l'Observation de la Terre (SPOT) satellites were archived as part of the 1990 Hawaiian Rainband Project (HaRP) and form the basis of the comparisons. During HaRP, GOES geostationary satellite coverage was marginal, so the main emphasis is on the polar-orbiting satellites.

1. Introduction

The first cloud pictures from orbiting satellites offered only a hint of the importance that they would play in modern meteorology (Hill 1991). These initial pictures from space were relatively low resolution and often appeared to be distorted by the underlying curvature of the earth. Nevertheless, they started a revolution in how we look at earth's weather, and even how we think of ourselves and our place on our planet. Over the intervening years, satellite images have increased in reliability and resolution. Using modern workstations images can be easily navigated and converted to a variety of standard map projections. In every sense, satellite data have become an essential component of our global observational network (Rao et al. 1990).

Initially, satellite observations were exclusively directed toward larger-scale synoptic features. With increasing sensor resolution, however, it became obvious that satellite imagery contained a wealth of information about smaller-scale features as well. In the United States, applications of satellite data to mesoscale studies (e.g., Fujita et al. 1968; Purdom 1976; Shenk et al. 1987; Rao et al. 1990[1]) have concentrated on data from geostationary satellites. There are a variety of polar-orbiting satellites, however, that offer additional capabilities and different perspectives that can play an important role in mesoscale meteorological studies (e.g., Cloakley et al. 1987; Isaacs and Barnes 1987; Scorer 1990).

In addition to providing daytime and nighttime cloud imagery and storm surveillance, operational satellites routinely collect temperature and moisture soundings to initialize numerical models. Research satellites likewise collect an amazing variety of remote sensing measurements. For mesoscale meteorological studies, however, the availability of high-resolution cloud imagery is often critical. In this paper we will examine the properties and capabilities of imagery from a variety of meteorological and environmental satellites. The focus will be on the highest-resolution imagery, primarily from polar-orbiting satellites. In particular, we will make extensive use of the digital datasets collected over the Hawaiian Islands during the Hawaiian Rainband Project (HaRP).

The HaRP was conducted during July and August 1990 on the island of Hawaii. The main focus of the experiment was the offshore rainbands that form along the windward shore of the island, near Hilo. A separate but complimentary component of the project was concerned with the airflow in the lee of the island. The facilities used for the project included 1 meteorologically instrumented research aircraft, 2 C-band Doppler radars, and 50 portable automatic weather stations, all provided by the National Center for Atmospheric Research (NCAR). In support of the in situ measurement program, satellite data were collected from a number of sources. Unfortunately, only one Geostationary Operational Environmental Satellite

*Remote Sensing Facility, National Center for Atmospheric Research,++ Boulder, Colorado.
+Department of Oceanography, University of Hawaii, Honolulu, Hawaii.
**SeaSpace Corporation, San Diego, California
++The National Center for Atmospheric Research is sponsored by the National Science Foundation.
Corresponding author address: Remote Sensing Facility, National Center for Atmospheric Research, Boulder, CO 80307-3000.
In final form 8 July 1993.

[1]In particular, note chapter VII-8, "Convective Scale Weather Analysis and Forecasting."

(GOES) was operational during the project, and it was located far to the east. As the experiment started, however, an HRPT (high-resolution picture transmission) receiving station became available at the University of Hawaii and was used to archive data from the National Oceanic and Atmospheric Administration (NOAA) polar-orbiting satellites. With the cooperation of the U.S. Air Force, additional HRPT and DMSP (Defense Meteorological Satellite Program) imageries were collected at Hickam AFB on Oahu. In addition, arrangements were made with SPOT (Satellite Pour l'Observation de la Terre) image and EOSAT (Earth Observation Satellite Company), the commercial entities that manage and operate the SPOT and Landsat earth resources satellites to acquire imagery over the islands during the experiment. Subsequent to the project, limited datasets from the GOES satellite were obtained as well. In every case, the data were collected, archived, processed, and analyzed as digital imagery.[2]

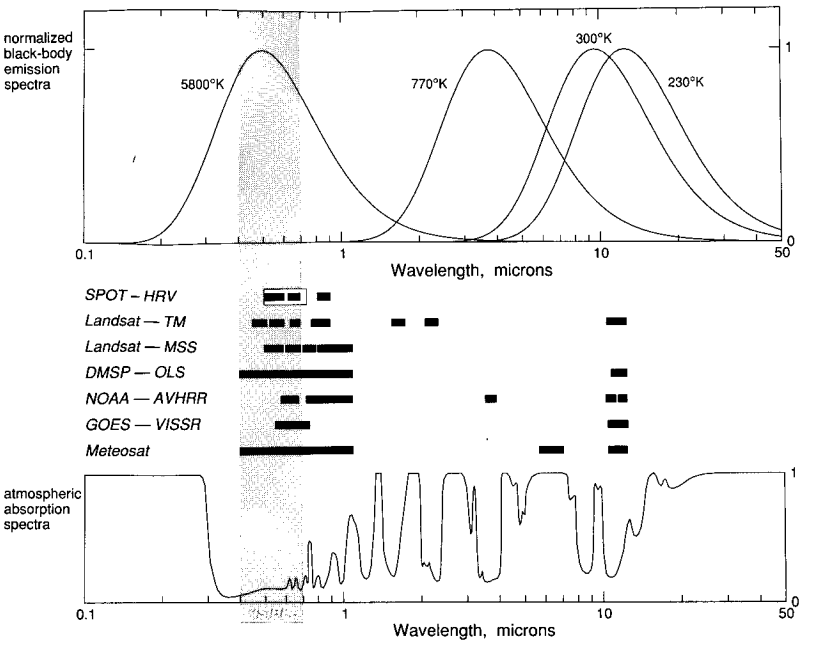

FIG. 1. Emission spectra, atmospheric windows, and satellite sensor response as a function of wavelength (after Scorer 1990; Goody 1964). Specific instruments include the Meteosat high-resolution radiometer, the GOES Visible and Infrared Spin Scan Radiometer (VISSR), the NOAA Advanced Very High Resolution Radiometer (AVHRR), the DMSP Operational Line Scanner (OLS), the Landsat Multispectral Scanner (MSS) and Thematic Mapper (TM), and the SPOT High Resolution Visible Imager (HRV). For each instrument, the black bars represent the wavelength interval detected by each separate sensor or data channel. In one case (SPOT), the imaging instrument can operate in both multispectral and panchromatic modes. In this case the broader panchromatic mode is delineated by a larger open "box" that encompasses the smaller black bars of the multispectral channels.

In order to understand the differences in the capabilities between the satellites used for meteorological studies, it is useful to consider the spectral sensitivity of the imaging instruments in the context of the expected locations of the peaks in solar and terrestrial emission spectra, as well as expected atmospheric absorption spectra (e.g., Scorer 1990). Figure 1 illustrates the spectral sensitivities of the imaging detectors for a wide variety of meteorological and environmental satellites. In every case, the imaging instruments collect multispectral data, that is, simultaneous images at two or more wavelengths. Most typically this is done at visible and infrared (IR) wavelengths. The bracketing plots surrounding the sensor information include a set of normalized blackbody emission spectra corresponding to both short wavelength solar emissions (5800 K) and longer wavelength terrestrial emissions (230, 300, and 770 K). The 230 and 300 K temperatures bracket the normal range of earth surface temperatures, while the 770 K corresponds to much warmer temperatures such as red-hot lava. In addition to the emission spectra, Fig. 1 also presents a typical atmospheric absorption spectra (Goody 1964). The absorption spectra highlights the various *windows* in which radiation is not absorbed by the atmosphere. Satellite observations are normally constrained to one or more of these window regions. The 6.5-μm "water vapor" channel on the Meteosat geostationary satellite is the sole exception presented in Fig. 1. This imaging channel is positioned squarely in the midst of a water vapor absorption band. The natural variability in atmospheric water contents, however, results in a variable degree of penetration of the atmosphere. The observed radiation, of course, is just the IR emissions from clouds and the atmosphere, with the specific brightness temperature reflecting the depth of penetration. The temperature patterns observed, therefore, indicate the overall distribution of cloudiness and water vapor in the middle and upper atmosphere. Visible light is in the range of 0.4 to 0.7 μm wavelength, squarely in the peak of the solar emissions, and is the most important window region for absorption. Visible images, at a variety of wavelength intervals extending into the near IR, form the primary core of high-resolution meteorological imag-

[2]A separate long-term archive of hard copy GOES imagery, including data obtained during HaRP, is maintained at the University of Hawaii but was not used in the current study.

ery. Thermal IR emissions from earth peak in the 10–12-μm window, where there is a secondary cluster of observations.

2. Geostationary satellites

Geostationary satellites orbit in earth's equatorial plane at a height of 35 800 km. At this height, the satellite's orbital period matches the rotation of earth, so the satellite seems to "hover" over the same point on the equator. Small imperfections in the orientation of the orbital plane and eccentricity in the orbit, caused in part by asymmetries in earth's gravitational field, causes the subsatellite point to drift, usually in a small oval or figure-eight pattern centered on the equator. Periodic station-keeping adjustments to the satellite's orbit can minimize these orbital deviations and maintain the subsatellite point to within about 1° in latitude and 0.5° in longitude. Eventually, all satellites will run out of hydrazine or the other propellents used for orbital adjustments, and the orbit will gradually deteriorate.

Since the field of view of a satellite in a geostationary orbit is fixed, it always views the same geographical area, day or night. This is ideal for making regular sequential observations of cloud patterns over a region with visible and IR radiometers. The high temporal resolution and constant viewing angles are the defining features of geostationary imagery.

Since the field of view of a satellite in a geostationary orbit is fixed, it always views the same geographical area, day or night. This is ideal for making regular sequential observations of cloud patterns over a region with visible and IR radiometers.

a. Geostationary Operational Environmental Satellite

As part of its operational meteorological satellite program, the United States generally maintains two geostationary satellites: one at 75°W, called GOES-East, and the other at 135°W, called GOES-West (Fermelia 1982; Clark 1983; Gibson 1984; World Meteorological Organization 1989; Rao et al. 1990). The main imaging device on the U.S. GOES satellites is the Visible and Infrared Spin Scan Radiometer (VISSR). This instrument takes advantage of the spin stabilization of the satellite to produce cloud images. The satellite rotates at 100 revolutions per minute (rpm). With each rotation, a high-resolution radiometer scans across the distant earth disk from west to east. With each rotation, a mirror steps down by 0.192 mrad (milliradian) (0.011°), so subsequent scan lines are displaced southward, until the scan is completed. The IR channel consists of output from one of two IR detectors, or an average of them both, each having a field of view of 0.192 by 0.192 mrad (equal to the north–south scan step). A fiber-optics bundle couples the radiometer telescope to an array of eight visible (VIS) detectors. These detectors are oriented perpendicular to the scan direction, effectively subdividing each line into eight parallel data streams. Each separate VIS detector has a 0.025 (E–W) by 0.021 (N–S) mrad field of view. At nadir, this corresponds to a VIS resolution of 0.9 km (E–W), as compared to an IR resolution of 6.9 km. Visible data are sampled every 2 μs, corresponding to an angular rotation of 0.021 mrad. The IR data are sampled every 8 μs, corresponding to an angular rotation of 0.084 mrad. VIS data are slightly oversampled, while the IR data are oversampled by more than a factor of 2. Visible data is quantized to 6 bits (64 levels), while the IR data are quantized to 8 bits (256 levels).

In the current generation of GOES satellites, the VISSR instrument has been enhanced with additional IR sensors that provide a capability for atmospheric soundings. The overall instrument is now formally named VAS (VISSR Atmospheric Sounder). In addition to a variety of dwell-sounding capabilities, the enhanced VAS instrument permits some additional multispectral imaging capabilities. In the multispectral imaging mode, it is possible to collect and transmit data from up to three different IR channels, in addition to visible imagery. In this case, the instrument resolution, at nadir, is roughly 1 km for the visible channel and 13.8 km for the IR channels. While these additional IR channels are relatively low resolution, the 6.7-μm IR channel has come into widespread usage to map upper-tropospheric moisture patterns. When operating in VISSR mode, the basic high-resolution imaging capabilities are unchanged from earlier satellites. In Fig. 1, only the two traditional VISSR viewing channels have been plotted.

For a given satellite and orbit, it is usually a straightforward geometric exercise to calculate the sensor resolution, sampling frequencies, and viewing angles relative to earth's surface. Figure 2, for example, illustrates the sensor resolution and sampling frequency for VISSR visible data. As the radiometer scans away from nadir, the effective resolution of the data is decreased due to the curvature of the earth and

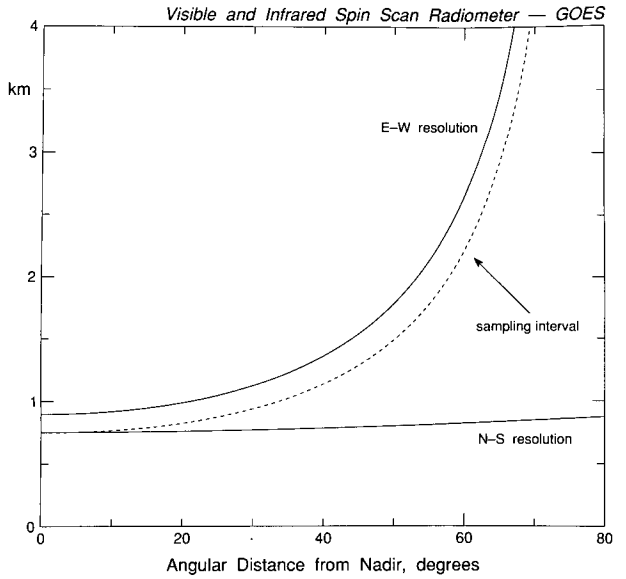

FIG. 2. Sensor resolution and sampling interval for the GOES Visible and Infrared Spin Scan Radiometer. This figure is based on an equatorial scan but is broadly representative of the resolution reductions expected for other scans as well.

the increasing distance to the satellite. The major reduction in sensor resolution, of course, is in the direction of earth's curvature. In the other direction, the only effect is the increasing distance to the satellite, a relatively minor effect from geostationary altitudes. While the computations were explicitly performed for a scan along the equator, the overall degradation in effective resolution indicated in Fig. 2 is applicable to any great circle arc passing through the subsatellite point. Infrared data, of course, undergoes an analogous degradation with distance from nadir as well.

From geostationary altitude, earth only subtends an angle of slightly more than 17 degrees. To ensure that a "whole disk scan" covers the entire earth field of view (a great circle arc of slightly more than 80 degrees), the VISSR scans a 20° by 20° area, with a full set of scans (1821 in all) taking about 18.2 min. Although each image takes a relatively long time to scan, the image is usually given a single time "stamp," based on the *start* of the scan sequence. Figure 3 illustrates the time offset between the beginning of a scan and the actual observations at any latitude. When two GOES satellites are operational, the eastern satellite begins its scan sequence on the hour and the half hour, while the western satellite begins its scans a quarter before or a quarter after the hour.

Except for a full disk scan every three hours, to coincide with global synoptic observations, the GOES scans are virtually never permitted to complete the full scan sequence. Most of the time, the scan is stopped after about 15 min (by which time the scan will have reached 40°S latitude) to permit dwell soundings or other operations. At other times, usually during outbreaks of severe convective storms, VISSR imagery is obtained more frequently, on intervals ranging from 15 min to as short as 3 min. In each case, however, the more rapid scan cycle is obtained at the cost of restricting the latitude limits for the scan. From Fig. 3, however, it is apparent that scan intervals as short as 3 min would be able to cover most of the United States. No matter how much the latitude limits of the scan are restricted, however, the spin scan radiometer always collects a full disk scan in the east–west direction.

High-resolution GOES imagery can be collected in real time by any site capable of receiving the "stretched" VISSR retransmission from the GOES satellite (see Rao et al. 1990). Historically this has been viewed as a relatively expensive and difficult proposition, but advances in workstation technology and high density storage media have made this an increasingly attractive way to obtain data. Alternately, a full digital archive of VISSR imagery is maintained at the Space Science and Engineering Center (SSEC) at the University of Wisconsin—Madison, and specific images can be obtained retrospectively from the archive.

Figure 4 (top panel) shows a VISSR visible image of the Hawaiian Islands obtained by *GOES-7* at 2005 UTC 21 July 1990. For this figure, the data have been digitally processed to a Cartesian latitude–longitude grid. All eight of the major Hawaiian Islands are visible in the image (highlighted by a coastline overlay). Moving from northwest to southeast, the islands are Niihau, Kauai, Oahu, Molokai, Lanai, Maui, Kahoolawe, and Hawaii. During the summer months, the trade winds blow regularly from east to northeast. In this image, there is a shield of cloudiness along the upwind sides of the islands from Hawaii to Oahu, along with

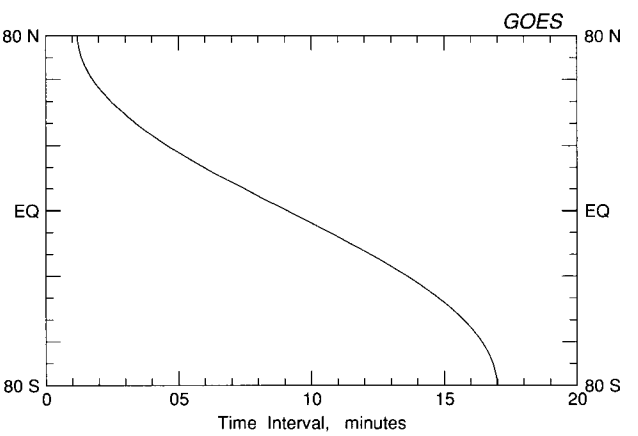

FIG. 3. Time interval in minutes between the start of a GOES VISSR scan sequence and the actual scan time at any specified latitude.

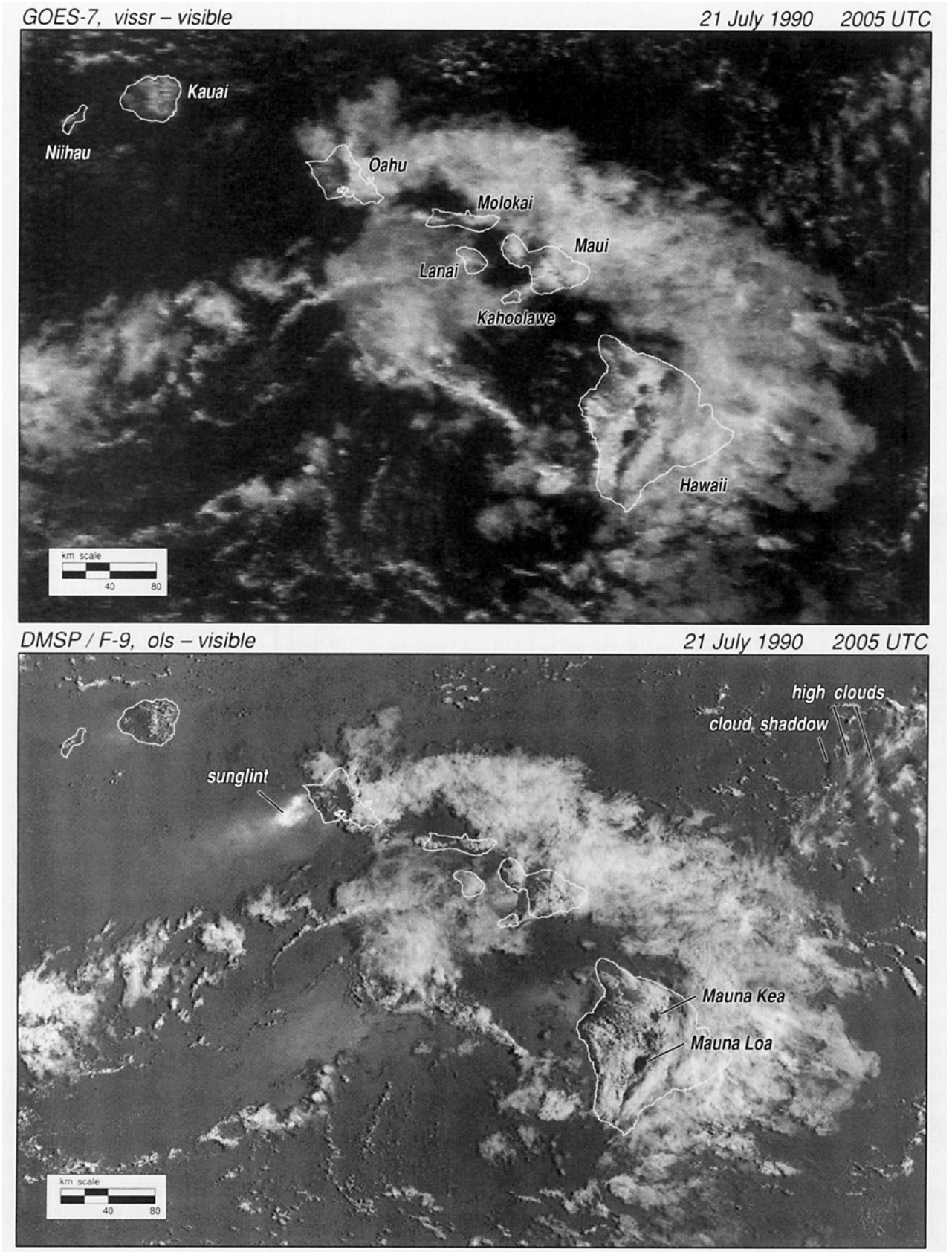

FIG. 4. Visible images of Hawaiian clouds taken from the *GOES-7* VISSR (top panel) and the DMSP/*F-9* Operational Linescan System (OLS) (bottom panel). Both images were obtained on 21 July 1990 at 2005 UTC.

considerable cloudiness over the islands as well. A complex string of clouds, apparently caused by the interaction of the islands with the trade winds, extends downwind from Maui, Lanai, and Molokai to the edge of the image. At the time of the observation *GOES-7* was at 98°W. This is very near the limit of useful data from a geostationary satellite, roughly 60° away from nadir. This is reflected in the relatively poor spatial resolution in the cloud imagery, which can be estimated from Fig. 2 to be about 3 km. In spite of the somewhat degraded resolution, the cloud patterns are quite distinct and even rather small clouds can be seen clearly.

The bottom panel in Fig. 4 is a simultaneous image collected by the *F-9* satellite from the DMSP (see section 3b). DMSP imagery is significantly higher in resolution than GOES imagery and is collected from satellites in low earth orbit. While *GOES-7* was far to the east at its geostationary altitude, the DMSP orbit passed to the west of the islands. Looking eastward, toward the midmorning sun, the DMSP image includes areas of reflected sunlight or sunglint. This lightens the apparent color of the ocean and can result in bright specular reflections in the calm water in the lee of the islands. Such reflections are visible downwind of Oahu and Maui and could on occasion be mistaken for clouds. In addition to the sunglint, there are distinct cloud shadows visible in the DMSP imagery that are difficult or impossible to detect in the GOES image. While the overall cloud patterns in the two images agree quite closely, it is also evident that the smallest clouds appear somewhat larger in the GOES image. The higher-resolution DMSP sensor, coupled with sunglint and shadows, also gives a three-dimensional appearance to the DMSP image.

In addition to the reduction in resolution with distance from nadir, the oblique angle from which the clouds are being viewed can result in a significant displacement in their apparent location. This parallax-induced cloud displacement is a function of the viewing angle and the height of the cloud above the ground. Figure 5 illustrates the normalized cloud offset for GOES, or any other geostationary satellite, due to this effect. For a cloud at any given height, the offset is just the height of the cloud, expressed in any desired units, multiplied by the normalized offset value from the graph. The direction of the apparent offset, of course, is directly *away* from the satellite along a great circle arc from the subsatellite point. Figure 4 is a good example of the parallax-induced cloud displacements. Since the GOES satellite was far to the east, there is a shift to the west in the apparent cloud positions as seen by GOES. Since the DMSP satellite passed to the west of the islands, its imagery contains a similar shift in apparent cloud locations, but in the opposite direction. For low clouds, the relative displacements are rather minor. For higher clouds, such as the cirrus visible in the northeast corner of the two images, however, the apparent displacements are clearly noticeable. This offset, of course, also applies to elevated terrain features, such as mountain peaks. This can be observed in the relative displacement of the visible location of the peaks of the two large volcanoes (Mauna Loa and Mauna Kea) that extend above the cloud cover over the island of Hawaii.

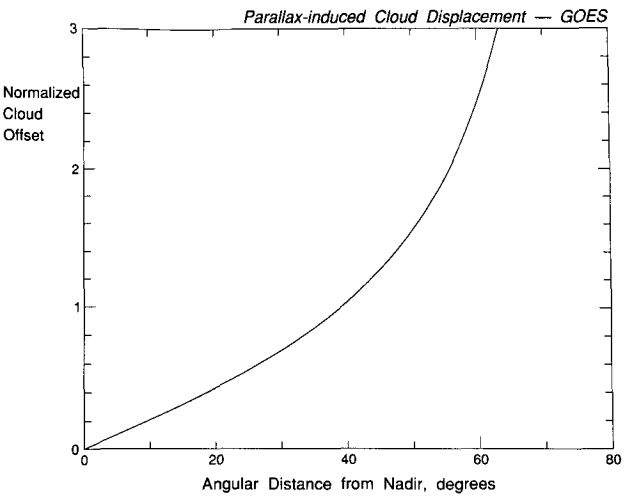

FIG. 5. Parallax-induced cloud displacement from geostationary orbit, as a function of the angular distance from nadir. The cloud displacement is expressed in terms of its apparent offset from its true position, normalized by the height of the cloud.

b. Other geostationary satellites

In addition to the two geostationary satellites normally deployed by the United States, additional geostationary meteorological satellites are operated by the European Space Agency, the Japan Meteorological Agency, and the Indian Space Research Organization (Massom 1991; World Meteorological Organization 1989; Rao et al. 1990; Mason and Schmetz 1992; de Waard et al. 1992). The Japanese Geostationary Meteorological Satellite (GMS) is deployed over the western Pacific at 140°E. The current satellite in this series is designated *GMS-4.* The European geostationary satellite Meteosat is deployed along the Greenwich meridian. The satellite in this series is *Meteosat-5.* With the delayed launch of the next GOES satellite, the older *Meteosat-3* satellite has been moved to 75° W to give improved coverage of the Atlantic (de Waard 1993). The Indian National Satellite System (INSAT) is an operational multipurpose satellite designed to support communications, television broadcasting, and meteorological observations. The INSAT satellite is positioned at 74°E.

GMS and Meteosat are generally similar to the

GOES satellites, but with some important differences. Like GOES, both GMS and Meteosat are spin-stabilized satellites with a nominal spin rate of 100 rpm. In all three cases, cloud imagery is obtained by a variant of a spin scan radiometer. The angular step for each GMS or Meteosat scan line, however, is 0.140 mrad (0.008°), a bit finer than that employed by GOES. This means that a 20° by 20° scan will take about 25 min. For both satellites the IR sensors have angular fields of view of 0.140 mrad. At nadir, this corresponds to a resolution of 5 km. Like GOES, the visible resolution is enhanced by subdividing each scan line by a linear array of smaller visible detectors. For Meteosat, each scan line is split by two visible sensors perpendicular to the scan direction. For GMS, each scan line is split by four visible sensors. This means that at nadir, the nominal visible resolution of Meteosat is only 2.5 km, while for GMS the nominal resolution is 1.25 km. Like GOES, GMS quantizes the IR data into 256 levels (8 bits), while the visible data only has 64 levels (6 bits). For Meteosat, both VIS and IR data are encoded into 256 gray levels (8-bit data). In addition to the thermal IR channel, Meteosat also collects imagery in the 5.7- to 7.1-μm water vapor absorption band. Like the corresponding thermal IR data, this channel has a resolution of 5.0 km, with an 8-bit quantization.

INSAT is currently the only three-axis stabilized geostationary meteorological satellite. Its imaging device is a two-channel Very High Resolution Radiometer (VHRR), operating in the visible (0.55–0.75 μm) and infrared (10.5–12.5 μm) wavelengths. At nadir, the visible channel has a resolution of 2.75 km, while the IR channel has a resolution of 11 km. The VHRR instrument can provide full earth coverage every 30 min and sector scans in as little as 5 min. In most cases, however, earth images are only collected at three-hourly intervals. Images are primarily archived as photographic prints, and digital data are notoriously difficult to obtain.

3. Polar-orbiting satellites

There are a number of polar-orbiting satellites that play an important role in meteorological and environmental remote sensing from low earth orbit. In this section we will examine four of these satellites: the NOAA satellites, the satellites of the DMSP, Landsat, and SPOT. All four satellite systems have almost identical orbital parameters but use quite different imaging instruments.

These satellites are all in near-polar circular sun-synchronous orbits. Their altitudes range between 700 and 800 km, with orbital periods of 98 to 102 min. The DMSP and NOAA satellites were designed for meteorological observations. Imagery from successive orbits overlap with each other, giving global daily coverage from each satellite. Landsat and SPOT, on the other hand, are intended for geophysical remote sensing, with an emphasis on high-resolution and multispectral imagery, at the cost of frequency of observation.

To achieve a sun-synchronous orbit, the orbital plane is inclined slightly away from a true N–S orbit in order to introduce a slow precession in the orbital plane (roughly one degree per day). This precession ensures that the equatorial crossing times of the satellites, in terms of the local solar time, remain nearly constant throughout the year. This means that a satellite can make repeated global observations from a single set of sensors with similar illumination from pass to pass. Unlike the geostationary satellites, the meteorological polar-orbiting satellites do not carry orbit maintenance propellant, and with time the orbits will drift away from their intended equatorial crossing times (Price 1991). The Landsat and SPOT satellites, on the other hand, do carry a supply of propellant for

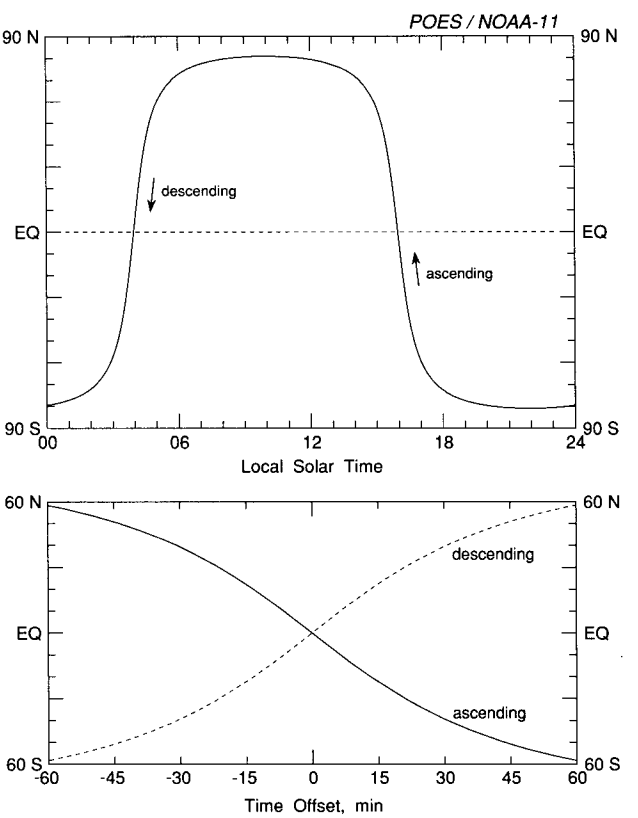

FIG. 6. An example of a near-polar sun-synchronous orbit (*NOAA-11*, July 1993). The curve shows the local solar time at the subsatellite point for one full orbit (upper panel). The lower panel shows the time offset in minutes from the equatorial crossing time for ascending and descending nodes.

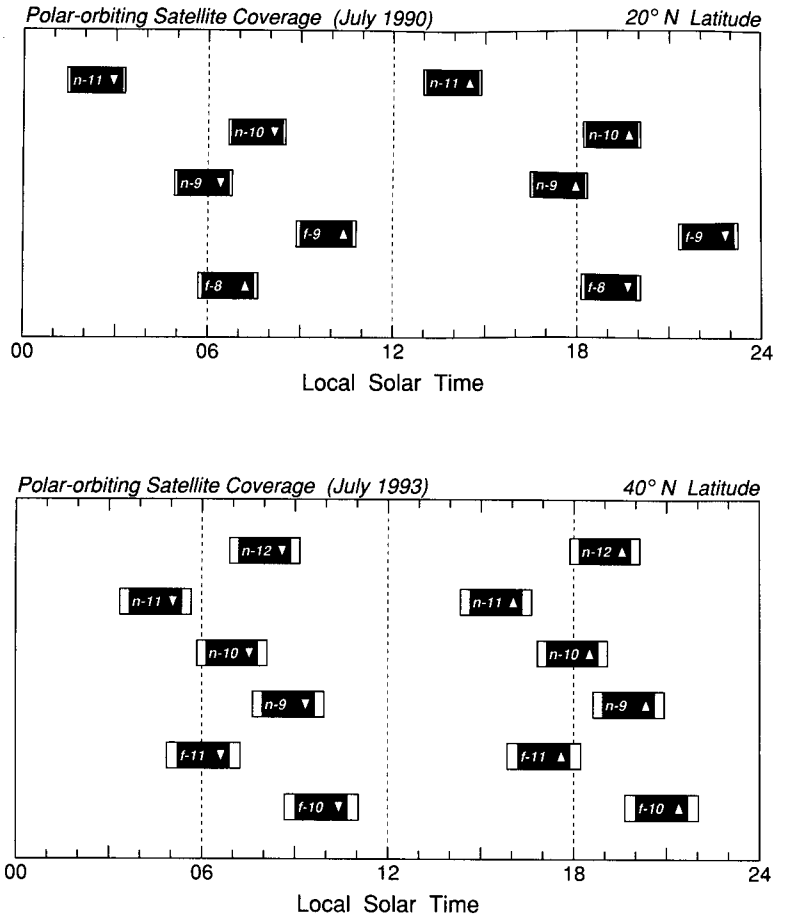

FIG. 7. Polar-orbiting satellite coverage (DMSP and NOAA) for July 1990 at 20°N latitude and July 1993 at 40°N latitude. In each case, the black bar indicates the range of times possible for each overpass. NOAA satellites are identified by an "n" identifier, while DMSP satellites are identified by an "f" designation. Triangles pointing up designate a satellite in an ascending node (moving from south to north), while a downward pointing triangle indicate a satellite in a descending node (moving from north to south).

making periodic orbital adjustments and can, therefore, maintain relatively constant equatorial crossing times over the satellite's operational lifetime.

Figure 6 illustrates some features of a near-polar sun-synchronous orbit. This specific example is based on the *NOAA-11* satellite, with orbital parameters from July 1993. The top panel tracks the local solar time (LST) at the subsatellite point throughout one entire orbit. The farthest poleward excursion of the satellite is at 81°N or S latitude. The equatorial crossing times are at 0400 and 1600 LST. While the equatorial crossing times are precisely 12 hours apart, consecutive passes at other latitudes are not evenly spaced in time. For the *NOAA-11* example, the satellite will cross 40°N latitude at 0431 and 1529 LST. The bottom panel of Fig. 6 shows the time offset from the equatorial crossing time as a function of latitude. Unlike the top panel, which, strictly speaking, is only applicable to a single satellite and date, the bottom panel is more general and gives a good first approximation of the anticipated time offset from the equatorial crossing time for each of the satellites discussed in this section. While sun-synchronous orbits will have consistent scene illumination from pass to pass, neither the local solar time nor the illumination angles will be the same at different latitudes. The solar illumination angles will also have a significant seasonal variation.

Ignoring any long-term drift, the time of a satellite pass, measured in local solar time at nadir, is constant for a given latitude. The time that a satellite makes its nearest approach to any given location, however, is not necessarily constant. All the polar-orbiting satellites discussed in this section, for example, have orbital periods that do not result in an integer number of orbits per day. This means that there is a natural precession from day to day, depending on the position of the satellite track relative to the point of interest. The Landsat and SPOT satellites attempt to maintain exactly repeating orbits, but the repeat periods are quite long (16 days for Landsat and 24 days for SPOT).

Figure 7 illustrates the range of possible pass times for NOAA and DMSP satellites. The top panel shows the satellites that were in operation during HaRP in July 1990. The bottom panel, for comparison, shows comparable data for the satellites in operation three years later. In this later case, the latitude of observation has also been changed to 40°N. In these figures, the time of nearest approach of the satellite will always occur within the time block indicated by the broad black bar. The width of the bar is equal to the orbital period of the satellite. Like Fig. 6, time is expressed in terms of local solar time, but in this case, the relevant time is that at a given latitude and longitude, not at a point moving with the satellite. After launch, NOAA satellites are given a sequential number and the name NOAA (shortened to "n" in the figure), while the DMSP satellites are normally identified with a number and the letter "f." The field of view and swath width of both the satellites are wide enough to permit full coverage at the equator. That is, the coverage from successive passes will meet or overlap. Moving poleward, the amount of overlap increases and the likelihood that a given location would be within view during two succes-

sive passes increases proportionally. In Fig. 7, the time periods during which a second pass might be seen are indicated by the white extensions to the black bars. The relative sizes of the white and black areas indicate the relative frequency of catching two consecutive passes as opposed to a single pass; for example, if the white areas were half as large as the black area, you would expect to have satellite coverage on successive passes every other day. By 60° latitude, the overlap is great enough that two successive passes are always in view. In addition to noting the differences in the observation times at different latitudes, Fig. 7 also shows the precession in the equatorial crossing times of the satellites during a 2-yr interval.

Like the geostationary satellites, the polar-orbiting satellites generally view clouds from an oblique angle, resulting in an apparent displacement in the location of the clouds relative to surface features. Figure 8 illustrates this parallax-induced cloud displacement for the DMSP and NOAA meteorological satellites. The critical parameter, of course, is the viewing angle of the satellite, relative to the local plane of earth's surface. This is a function of both the relative position of the satellite and the curvature of the earth. For geostationary satellites, the earth curvature term is by far the most important. For polar-orbiting satellites in low earth orbit, both terms are important. Relative to their respective fields of view, however, the errors in cloud positioning are quite similar.

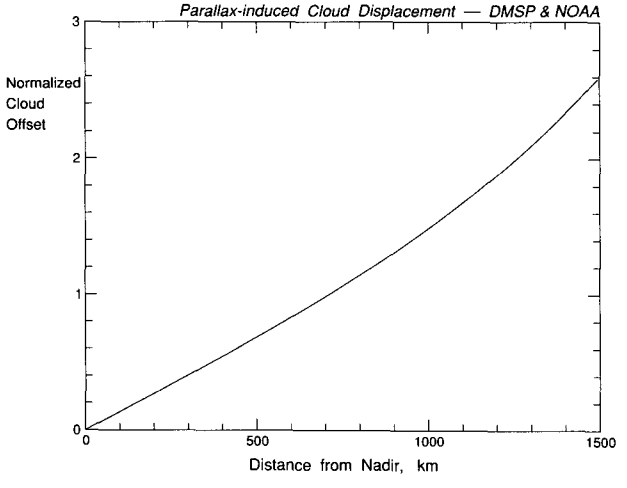

FIG. 8. Parallax-induced cloud displacement from low earth orbit (DMSP and NOAA satellites), as a function of the distance from nadir. As in Fig. 5, the cloud offset is expressed in terms of its apparent displacement from its true position, normalized by the height of the cloud.

a. NOAA meteorological satellites

The primary mission of the NOAA polar-orbiting satellites is to provide daily global observations of weather patterns and environmental conditions in the form of quantitative data usable for numerical weather prediction. The satellites are used to obtain estimates of cloud cover, ice and snow coverage, sea surface temperature, and vertical profiles of temperature and humidity (Rao et al. 1990). These satellites are part of the advanced TIROS-N (ATN) series of satellites (Schnapf 1982), under what is now termed the POES (Polar-orbiting Operational Environmental Satellite) program. The major imaging instrument on these satellites is the Advanced Very High Resolution Radiometer (AVHRR). In its most current version, this is a five-channel scanning radiometer with 1.1-km resolution (at nadir) in *each* channel. There is one visible channel, one near-IR channel, one channel in the middle IR, and two channels in the longer wavelength thermal IR region (see Fig. 1). Channels 4 and 5 are often referred to as "split channels." An older four-channel version of the instrument has a single thermal IR (10.5–11.5 μm) channel. For consistency, the transmitted data stream always contains five data channels, with the fifth channel of the four-channel instrument just containing a retransmission of the fourth channel data (Kidwell 1991). Of the satellites discussed in this section, *NOAA-9, NOAA-11,* and *NOAA-12* are equipped with the five-channel AVHRR instrument, while *NOAA-10* is the only satellite currently using the four-channel instrument. *NOAA-12* is the first "morning" satellite in the ATN series to carry the five-channel AVHRR instrument.

The primary mission of the NOAA polar-orbiting satellites is to provide daily global observations of weather patterns and environmental conditions in the form of quantitative data usable for numerical weather prediction.

Two polar-orbiting satellites are normally operational at any one time. They are placed in sun-synchronous orbits at altitudes of approximately 833 and 870 km. One satellite will have an early-morning equatorial crossing time at about 0730 LST (descending node), while the other will have a nominal equatorial crossing time of 1430 LST (ascending node). The intent, therefore, is to have one satellite observing the earth in the early morning and early evening and a second satellite making observations in the early afternoon and in the middle of the night. Data from the satellites is transmitted in real time, as well as being stored on-board the spacecraft for retransmission

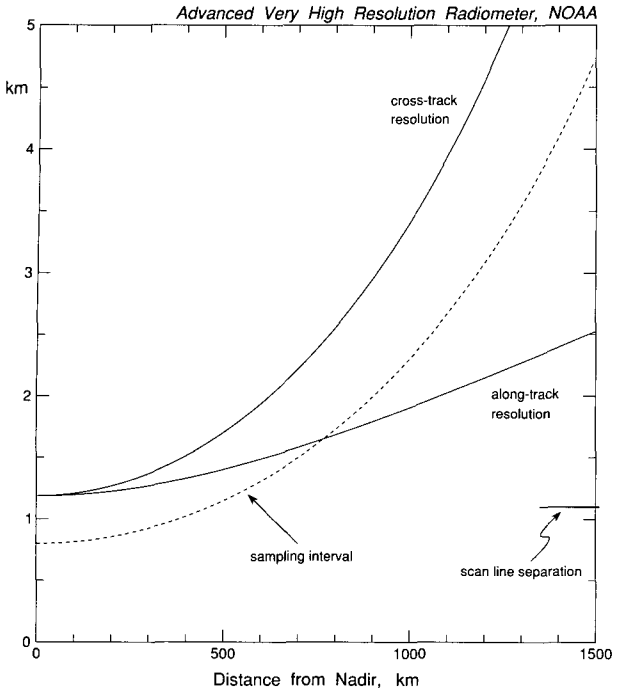

FIG. 9. Advanced Very High Resolution Radiometer sensor resolution as a function of distance from nadir.

over a command and data acquisition (CDA) station at Wallops Island, Virginia, or Fairbanks, Alaska. Direct transmission data is called HRPT (high-resolution picture transmission) and is broadcast at the full resolution of the AVHRR instrument. Data stored for retransmission include a reduced-resolution dataset (4 km at nadir) that covers the entire orbit, called global area coverage or GAC, and an optional area of full resolution data, called local area coverage or LAC. GAC data are always archived for the two "operational" satellites, while LAC data can only be collected over a limited portion of a orbit. In addition to the HRPT data stream, the NOAA satellites also transmit lower-resolution (4 km) data for two of the five channels by means of an analog APT (automatic picture transmission) broadcast that can be received by relatively inexpensive receiving stations.

The CDA stations are only equipped to handle data from the two operational satellites. In most cases, however, satellites will continue to broadcast HRPT data after they are no longer considered operational by the National Environmental Satellite Data and Information Service (NESDIS). During the 1990 Hawaiian HaRP project, three NOAA satellites were transmitting HRPT data. Two years later, a new operational satellite, *NOAA-12,* had been launched, raising the number of NOAA satellites transmitting HRPT data to a total of four. As shown in Fig. 7, morning passes are quite frequent, while the afternoons are only covered by the *NOAA-11.* This coverage disparity is the result of *NOAA-9,* originally an "afternoon" satellite, drifting into the morning.

The AVHRR instrument views the earth through a telescope and a rotating mirror. The mirror rotates at a constant 360 rpm to produce the cross-track scanning in orbit. The data are sampled every 25 μs with the transmitted data limited to a 2048 sample swath centered at the subsatellite point (Kidwell 1991). This results in a swath width of slightly less than 3000 km. The angular field of view of the radiometer optics is 1.3 mrad, corresponding to a resolution of 1.1 km at nadir. The orbital motion of the satellite causes each consecutive scan to be displaced by 1.1 km in the direction of the orbit. The curvature of the earth and the increasing slant distance to earth's surface, however, causes the effective resolution of the sensor to degrade significantly toward the edges of the scanned swath. The reduction in resolution near the edges of the pass are so significant that the swath width is frequently quoted as being a bit less that the actual area scanned by the instrument (e.g., Rao et al. 1990). Figure 9 illustrates the resolution of the AVHRR data as a function of distance from nadir. The main factor degrading the instrument's resolution is the curvature of earth. Since the satellite is looking at an increasingly oblique angle, the effective resolution of the sensor is progressively degraded as it moves away from nadir. The effects of earth curvature, however, are not uniform, but rather concentrated in the cross-track direction, that is, along the scan line. In the other direction, along the satellite track, the sensor resolution also degrades with distance from nadir, but only because of the increasing distance from the satellite (Flannigan and Vander Haar 1986; Breaker 1990). The scan-line separation is a constant 1.1 km, while the data within a scan line are slightly oversampled. Both HRPT and LAC datasets are transmitted with 10 data bits per pixel for each channel.

Figure 10 shows an example of a visible *NOAA-11* image, recorded at 0007 UTC 27 July 1990 (1407 LST). As is usually typical of summer afternoons, considerable cloudiness has built up over the islands. Like the DMSP image from 21 July (Fig. 4), there is evidence of sunglint in the calm waters in the lee of the islands. Of particular interest are the sharp boundaries to the areas of sunglint, particularly near the north end of the island of Hawaii. This feature is caused by a sharply defined and relatively permanent shear zone at the north end of the island (e.g., Smith and Grubisic 1993). To the north of the shear zone, the trade winds blow steadily through the Alenuihaha Channel between Hawaii and Maui, while to the south of the shear zone, the flow is relatively calm and may even be blowing onshore. The sharp discontinuity in the wind speed and direction is mirrored in the surface wave

structure, which in turn visibly modulates the sunglint pattern. In addition to the sunglint patterns, there are a number of interesting small clouds that have formed directly along the shear zone itself. Such features in the lee of islands can be quite striking and have received a great deal of attention in literature (e.g., Lyons and Fujita 1968; McClain and Strong 1969; Cram and Hanson 1974; Strong et al. 1974; Fett and Rabe 1976; Needham 1976; Fett and Burk 1981; and Langland et al. 1987).

While sunglint can often be considered a contaminant, it can also produce spectacular images with detailed structures in ocean surfaces. The intensity of the glint is primarily a function of the sea state, solar angle, and viewing angle of the satellite (Wald and Monget 1983; Rao et al. 1990). By relating sea state to wind velocity, it may be possible to use sunglint to extract estimates of the surface wind velocity (Khattak et al. 1991). In the HaRP imagery in particular, sunglint often highlights the shear zones in the lee of the islands that would otherwise not be visible.

An important feature of the AVHRR imagery is the uniform spatial resolution of the multispectral data (1.1 km at nadir). This greatly facilitates the development of multispectral algorithms, such as those used for sea surface temperature (Bernstein 1982; Robinson et al. 1984; McClain et al. 1985). Other applications of multispectral imagery include land use and vegetation properties (Lillesand and Kiefer 1987), cloud identification and classification (Arking and Childs 1985; d'Entremont 1986; Saunders and Kriebel 1988; Yamanouchi et al. 1987), contrail identification and enhancement (Lee 1989; Engelstad et al. 1992), and under some conditions, estimates of cloud droplet sizes or concentrations (Cloakley et al. 1987).

The AVHRR channel centered at 3.7 μm (channel 3) is of particular interest. This channel is midway between the shorter wavelength visible channels and the longer wavelength thermal IR. During daytime, it is very sensitive to reflected sunlight, while at night it behaves more like a normal IR channel (Scorer 1986b, 1990). While normal solar or terrestrial emission spectra are at a relative minimum at this wavelength (see Fig. 1), the channel is quite sensitive to heat sources such as fires or lava flows (e.g., Scorer 1986a; Lee and Tag 1990; Dousset et al. 1993). Figure 11 shows a nighttime channel 3 image of the island of Hawaii. The major features visible are the clouds, silhouetted as

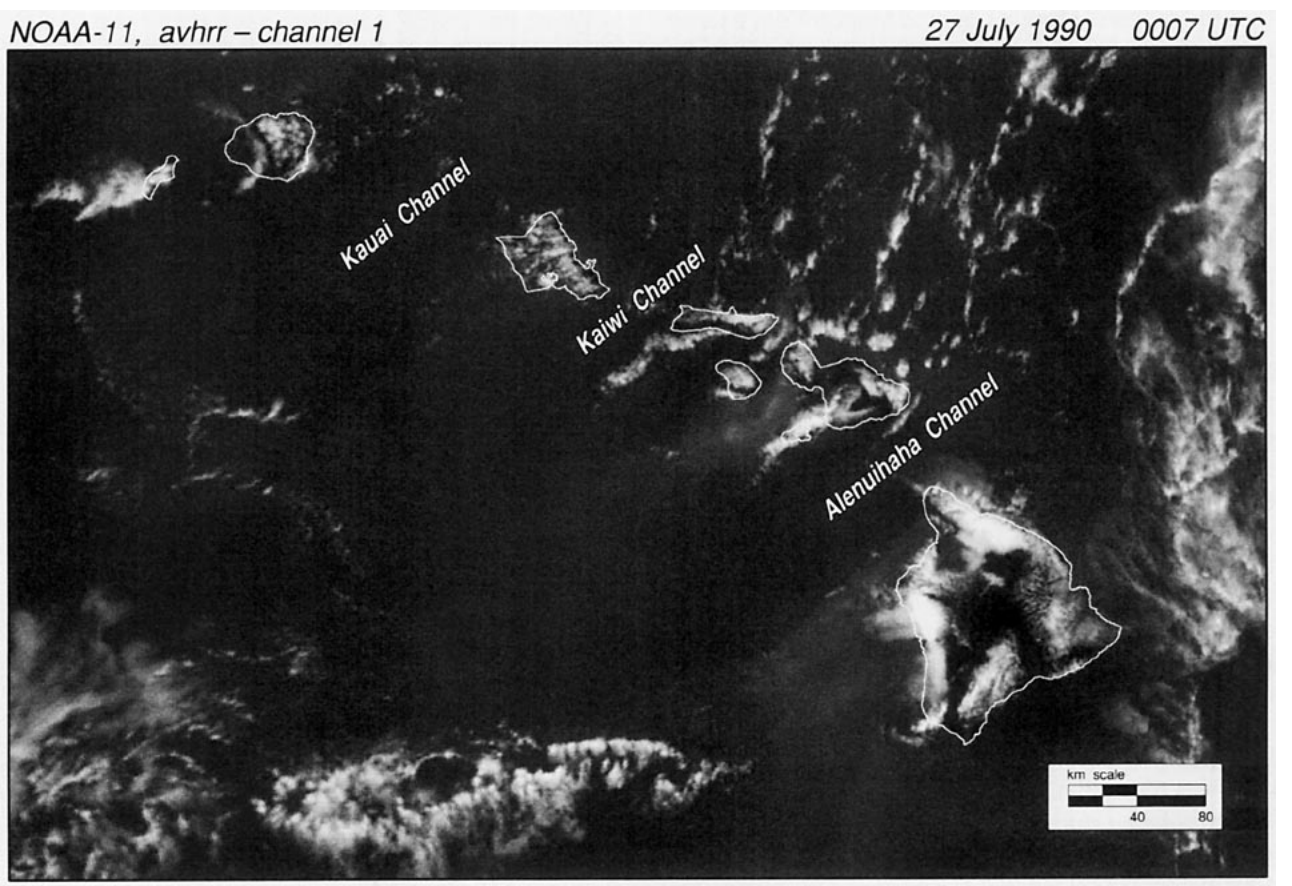

FIG. 10. *NOAA-11* afternoon image from 27 July 1990—AVHRR, channel 1.

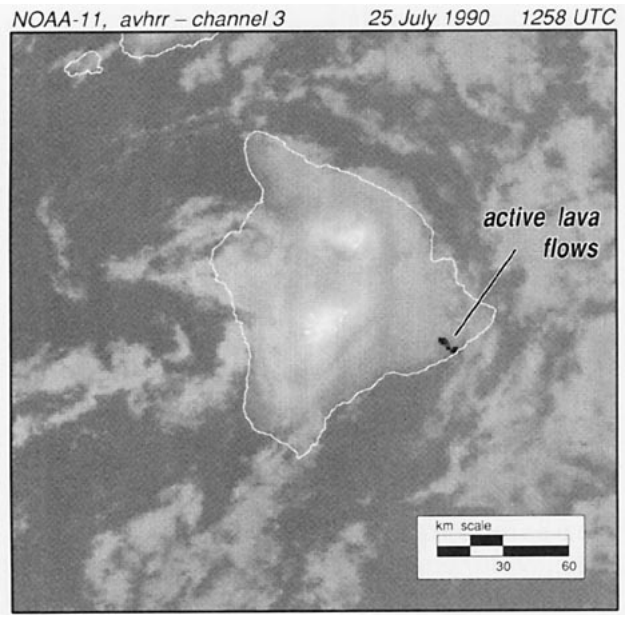

FIG. 11. *NOAA-11* nighttime near-IR image from 25 July 1990—AVHRR, channel 3. The bright spots along the southeast coast of the island of Hawaii are from an active lava flow on the flank of the Kilauea volcano.

cool features against the warmer sea, and the colder mountaintops of Mauna Loa and Manua Kea, extending well above the marine inversion. Against the relatively warm water, low clouds, if large enough, can be seen clearly in the nighttime IR data. At 3.7 μm, water clouds have relatively low emissivity. This means that at night, they may have brightness temperatures that are below their actual temperatures, increasing their contrast with the warm ocean surface. Over the island, it is more difficult to distinguish cloudy areas from the cloud free. Very small clouds, such as are apparently present in the channel between Hawaii and Maui, are difficult to resolve. The two black spots along the southeast coast of the island are images of the ongoing eruption of Kilauea that continued throughout the project. This image is quite typical, with two hot spots visible: one inland and one on the coast. The inland heat source is from the Pu'u O'o vent and adjacent Kupainaha lava pond. The lava itself flows to the sea through a system of underground lava tubes, only breaking out when it reaches the sea near Kalapana, and producing the second hot spot in the imagery.

b. DMSP meteorological satellites

Since the mid-1960s the U.S. Department of Defense has operated its own set of polar-orbiting meteorological satellites through the DMSP (Meyer 1973; Rivers and Arnold 1982; Goyette et al. 1990; and Klein et al. 1992). The DMSP satellites are primarily an operational system, with the direct broadcast transmissions encrypted. Until quite recently, the main operational product was a film-based hard copy, and digital data was difficult or impossible to obtain. In recent years, however, DMSP data have begun to become available to the meteorological community. Beginning on a limited basis in 1985, and continuously since 1987, DMSP transmissions over Antarctica have been transmitted without encryption. Since 1990, digital DMSP data have been collected in the Antarctic and are available from the Antarctic Research Center, along with digital AVHRR imagery dating back to 1987 (Van Woert et al. 1992). With the cooperation of the Department of Defense, DMSP data have also been acquired in support of a number of recent meteorological research projects, including the 1990 HaRP project, the 1991 Convection and Precipitation Electrification Experiment (CaPE) in Florida (Williams et al. 1992), and the 1992 Arctic Lead Experiment (LEADEX) in Alaska.

DMSP satellites are launched into near-polar sun-synchronous orbits at a mean altitude of about 835 km, an orbital inclination of 98.8°, and an orbital period of 101–102 min. The viewing swath is slightly broader than that of the NOAA satellites, often exceeding 3000 km (Hollinger et al. 1990; Massom 1991).

While the DMSP satellites have many similarities with the NOAA satellites, they also have a number of unique features and instruments that are not duplicated in other systems. One of the most important of these instruments is the SSM/I (Special Sensor Microwave Imager). This is a seven-channel low-resolution imager (15 to 50 km, depending on the wavelength) that can be used to generate a variety of geophysical parameters (see Goyette et al. 1990; Hollinger et al. 1990). In this context, however, the most important instrument on the DMSP satellites is the Operational Linescan System (OLS). The OLS is the DMSP's high-resolution imaging device for visible and IR radiation. The OLS instrument actually consists of a number of different sensors that can be operated in a variety of modes. The primary design goal of the daytime visible sensor is to obtain the highest-resolution imagery possible, consistent with reasonable data transmission rates and daily global coverage. The most significant feature of the instrument, however, may be its ability to maintain its high-resolution capabilities over virtually the entire swath width.

The OLS instrument continually points toward the earth, while being scanned back and forth in a sinusoidal motion. Successive scans are therefore made in opposite directions. The angular scan rate is most rapid at nadir and slows down as it approaches the end of its scan swath. With a constant sampling rate, this tends to maintain a relatively constant surface velocity

and a uniform sampling interval. Active adjustments are made during the scan to compensate for the sinusoidal scan pattern and to ensure that successive scan lines are parallel, straight, and perpendicular to the satellite track. The visible detector itself consists of an irregularly shaped segmented sensor that is rotated while it is being scanned. Through a sophisticated combination of sensor geometry and rotation rate, the effective sampling area of the sensor is reduced as it moves away from nadir, tending to maintain its high spatial resolution (Fett et al. 1983). Figure 12 shows the OLS visible sensor resolution as a function of distance from nadir. At nadir, the daytime OLS visible resolution is 550 m. As was the case with the AVHRR instrument, there is a constant separation between sequential scan lines that is roughly equal to the sensor resolution at nadir. Unlike the AVHRR instrument, however, the OLS cross-track sampling interval varies only slightly over the full swath width and is always less than the scan-line separation. The "nominal" sensor resolution, taken from Fett et al. (1983), does degrade as it moves away from nadir, but much less so than for AVHRR (cf. Fig. 9). About 730 km from nadir, one of the segments in the visible sensor is "turned off," effectively reducing the sensor size with an associated jump in resolution. To maintain image quality while the sensor is undergoing these changes, the OLS makes extensive use of a variable gain control. The variable gain feature also facilitates collection of useful imagery over a wide variety of ambient lighting, while only requiring 6-bit quantization. The OLS visible detector covers a much broader wavelength band than either of the AVHRR visible channels. On occasion, this difference in spectral response (see Fig. 1) can result in surprising differences in the imagery recorded by the DMSP and the NOAA satellites (e.g., Fett and Isaacs 1979).

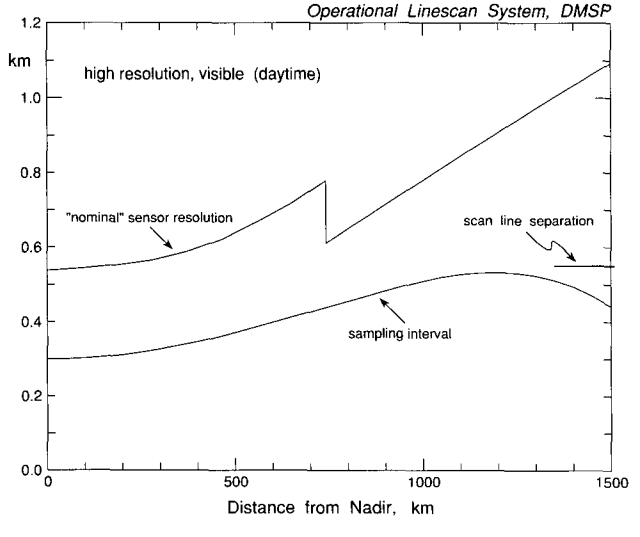

FIG. 12. DMSP Operational Linescan System daytime visible sensor resolution as a function of distance from nadir.

As indicated in Fig. 1, the OLS has both a visible and an IR channel. Like the daytime visible detector, the IR detector is an irregularly shaped segmented sensor. In the IR case, however, the segments are only switched at nadir. Rotation of the rectangularly shaped sensor tends to preserve the effective sensor resolution across the viewing swath, but without the pronounced jump in the resolution at 730 km from nadir. Like the visible channel, the IR resolution at nadir is about 550 m. The telemetry system, however, can only transmit one channel of high-resolution data, and the effective daytime IR resolution is degraded or "smoothed" to 2.7 km by on-board digital averaging of the data. Smoothed data are transmitted with 8-bit accuracy.

During nighttime passes, the sensor configuration is usually reversed (Foster and Hall 1991). In this case, visible data is usually transmitted in the lower-resolution smooth mode, and the IR data is transmitted at full resolution, as 6-bit data. The nighttime visible data is obtained with a high performance photomultiplier tube (PMT) using "light enhancement" technology. The PMT has somewhat different spectral characteristics than the daytime visible sensor and is electronically controlled to maintain its resolution across the image swath. Using this sensor, clouds and land areas can be viewed by visible light under a quarter moon or brighter. City lights can also be viewed quite clearly, with or without a moon.

Figure 13 shows a very early morning image of the Hawaiian Islands. Small convective cells dominate the image, along with a few regions of relatively thin cirrus (for example, between Hawaii and Maui). The areas in the lee of the islands tend to be relatively cloud free, with the exception of the long streamers of clouds that extend several 100 km downwind of several of the islands. There is an impressive set of wave clouds over Oahu, parallel to, and downwind of, the Koolau Mountain Range along the windward shore. There is an arc of clouds forming a "bow wake" on the eastern end of Maui, and what is apparently a solitary wave or roll cloud along the Kohala Peninsula on the north end of the island of Hawaii. The high-resolution OLS imagery is particularly well suited for viewing this sort of small-scale complex cloud structures.

Figure 14 shows another high-resolution visible image of Hawaii. In this case, the satellite passed to the west of the islands, a prime position to get sunglint in the image. Although still a morning image, this image is quite comparable to the afternoon *NOAA-11* image shown in Fig. 10. Many of the cloud features are similar, including the presence of small clouds forming along the shear lines that are dramatically illuminated

by the sunglint. As compared to Fig. 10, the increased resolution of the DMSP imagery is quite apparent. Even the dark lava flows on Mauna Loa are clearly visible in the OLS image.

On 18 August, we recorded virtually simultaneous AVHRR and OLS images, demonstrating the appearance of the images at the edges of their respective viewing swaths (see Fig. 15). Areas outside of the respective scan swaths are shown in black. The *NOAA-10* satellite passed 1412 km to the west, while the DMSP *F-9* satellite passed 1487 km to the east. The resolution differences emphasize the ability of the OLS sensor to maintain its effective resolution over its full swath width. While Figs. 10 and 14 put the AVHRR and OLS instruments in their best light, Fig. 15 shows a worst case comparison. The extremely disparate viewing angles makes some noticeable displacements in clouds in the two images. The low cloud directly west of Lanai, for example, appears to extend over the island in the NOAA imagery, while it seems clearly displaced to the west in the DMSP imagery. Even more interesting is the small patch of cirrus clouds located south of Maui and west of Hawaii. In the NOAA imagery, the shadow of the cirrus is just barely visible. With a knowledge of the satellite viewing angle and angle to the sun, the relative offset of the cloud and its shadow can be used to estimate the height of the cloud. The imagery is so blurry, however, that only a rough estimate of about 10-km height can be made. In this case, however, the height can be further refined by comparing the apparent position of the cloud itself in the two images. In this case we need only to know the viewing angles from each satellite, resulting in an estimated cloud height of just under 11 km. By a similar process, the clouds to the west of Lanai can be estimated to have a height of 2 km.

The variable gain feature of the OLS instrument permits imagery collection across the terminator at sunrise and sunset. Figure 16 shows a sunset image of Hawaii from 11 August 1990. The overlay shows the calculated sunset line (at the surface), along with the time before or after sunset across the image. For a setting sun, elevations above sea level will delay the local sunset. In general, an elevation of 1 km will effectively retard sunset by 5 min. In this example, the setting sun directly illuminates the tall streamer clouds in the lee of Hawaii, as well as the cloudiness along the Kona coast on the west side of the island. A double

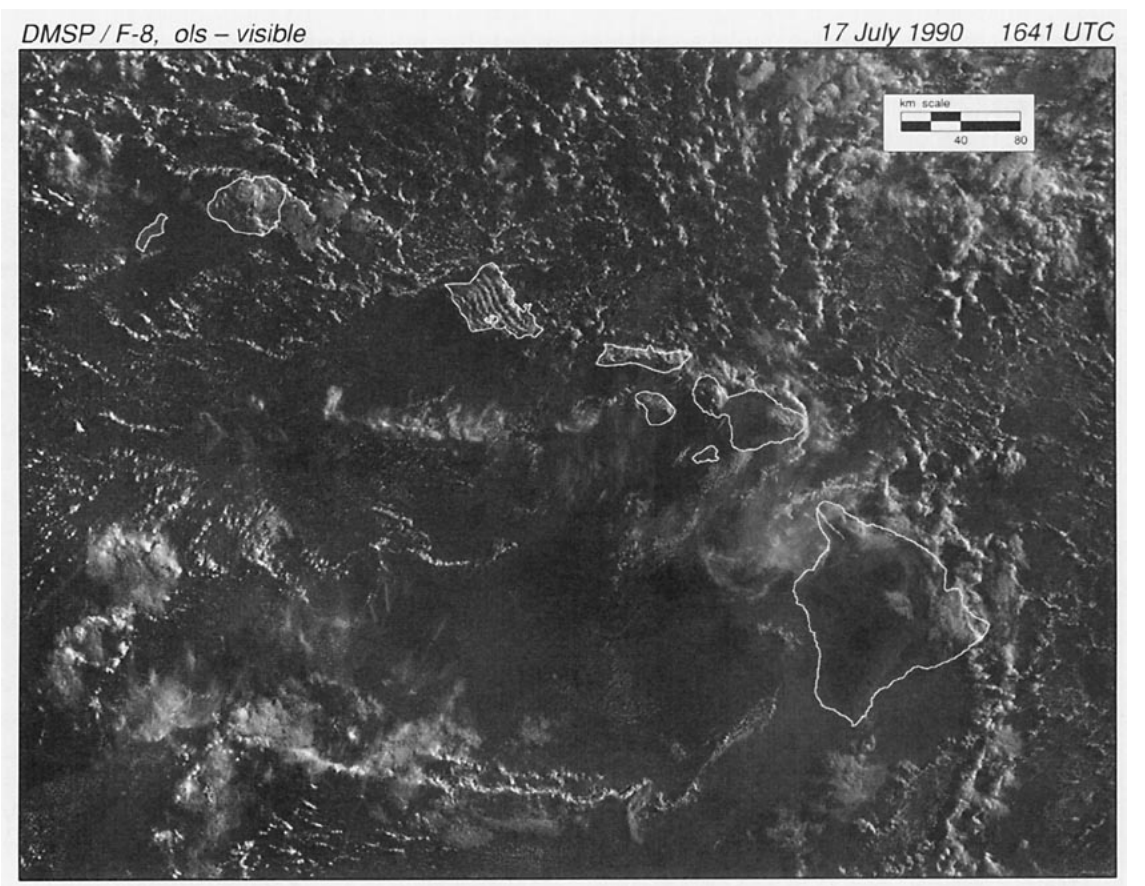

FIG. 13. An early-morning (0641 LST) OLS visible image of the Hawaiian Islands on 17 July 1990.

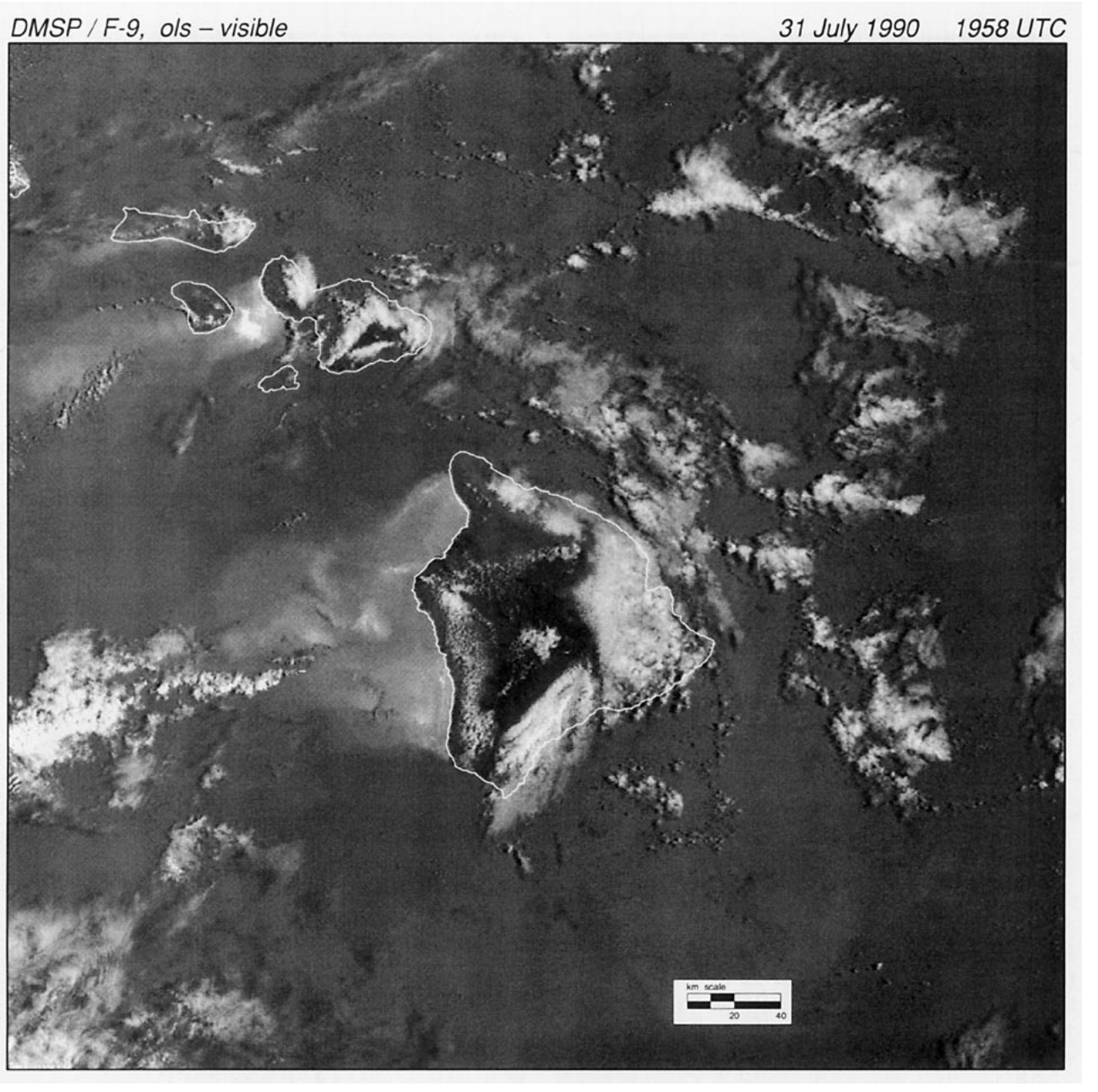

FIG. 14. A daytime high-resolution visible image from the OLS on the DMSP satellite *F-9*. This image was taken at 1958 UTC 31 July 1991. Patterns in the sunglint areas reveal details of the wind fields in the lee of the islands.

cloud line is visible along the northeast coast of the island, with only the tops of the clouds still receiving solar illumination directly. To the east, darkness sets in and the OLS instrument has to increase its gain to maintain an image, with an apparent increase in the background noise level.

Figure 17 shows a pair (VIS and IR) of nighttime images from 8 August 1990 (2141 LST on the 7 August). The top panel shows the high-resolution IR image, while the lower panel shows the visible image from the low-light PMT system. These images were taken two hours after moonrise, so the moon (two days after being full) was still relatively low in the sky. Nevertheless, the overall cloud patterns can be seen quite clearly. One interesting difference in the IR and visible imageries is the area of thin cirrus south of Hawaii. This cirrus is easily identifiable in the IR data but is not seen in the nighttime visible image. In addition to the clouds, lights are visible from Honolulu (on Oahu) and Kahului (on Maui). The eruption on the flank of Kilauea is also visible in the PMT imagery, more so than in the thermal IR data.

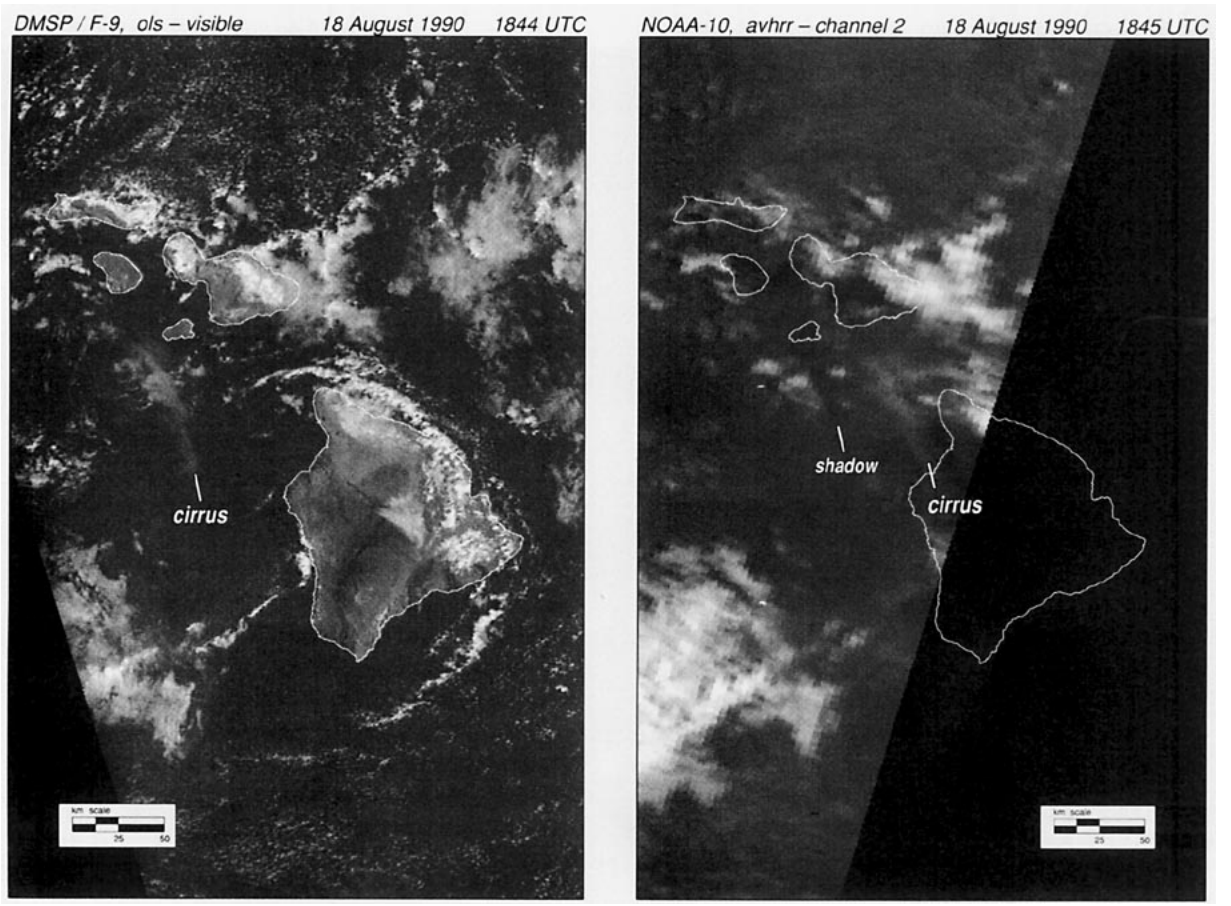

FIG. 15. A near simultaneous pair of images from DMSP and NOAA satellites. The images are both at the very edges of their respective viewing swaths.

c. Landsat environmental satellites

In parallel to the development of the operational polar-orbiting meteorological satellites of the TIROS series, the United States also operated a separate series of Nimbus research satellites (Eden et al. 1993).One of the developments of this research effort was a family of environmental or Earth Resources Technology Satellites, now known as Landsat (Haas and Shapiro 1982; Hill 1991). The primary mission of the Landsat satellites is high-resolution multispectral mapping of the earth's surface. Landsat data is distributed as a commercial product by EOSAT.

Like both the DMSP and NOAA polar-orbiting satellites, the Landsat satellites are in near-polar sun-synchronous orbits. The currently active Landsat satellites are *Landsat-4* and *Landsat-5.* Both satellites are in circular sun-synchronous orbits at a nominal altitude of 705 km and orbital inclination of 98.2°. The orbital period is 98.9 min, with a repeat cycle of 16 days. The two satellites follow the same orbital sequence, but eight days apart. So long as both satellites are operational, the effective repeat time is only eight days. An additional satellite, *Landsat-6,* with somewhat different capabilities is scheduled to be launched in the near future (see section 4).

There are two main imaging instruments on the current generation of Landsat satellite: the multispectral scanner (MSS) and the thematic mapper (TM). The TM is an extension of the MSS design, with improved spatial resolution and a wider range of multispectral information (see Fig. 1). Both imaging instruments are based on an object plane scan mirror. This mirror rocks back and forth to produce the cross-track scan, with the along-track component coming from the orbital motion of the satellite. MSS data are only collected from scans moving in a single direction (right to left, as seen from the satellite), after which the mirror rocks back to its original position to be ready for the next scan. In this case, a linear array of six detectors in each of the four spectral bands is aligned along the direction of motion of the satellite. This effectively subdivides the cross-track scanning area into smaller segments, much like what is done on the GOES spin scan radiometer. The effective field of view of each detector is approximately 79 or 80 m. During the cross-track scan, the sensors are

oversampled with the final digital dataset processed and delivered to the user with both cross-track and along-track sampling intervals of 57 m. Images are distributed as separate scenes, 185 km by 170 km. A variety of processing options are available but generally include a standard set of radiometric and geometric corrections. MSS datasets are quantized to 6-bit accuracy for transmission from the satellite and are processed and distributed as 7-bit (first three bands) or 6-bit (fourth band) data values.

A similar system is used to collect TM data, except in this case data are collected in both scan directions, and the rocking mirror collector is subdivided by 16 detectors per channel. This gives a ground resolution of about 30 m. The thermal IR channel is an exception. In this case, only four detectors are employed in the array, resulting in a ground resolution of roughly 120 m. All TM data are quantized to 8-bit accuracy. The final TM products are normally resampled to a pixel size of 28.5 m for path-oriented data, or 25.0 m for map-orientated datasets. In all cases, the lower-resolution thermal band is resampled to the same pixel size as the reflective bands.

Figure 18 shows an MSS image of Maui, Kahoolawe, and a major portion of the island of Hawaii.[3] The image had been corrected to remove geometric distortions but has been maintained in its natural orbital orientation, slightly tilted away from true north. The lava flows on Mauna Loa, as well as a variety of topographic features, are all clearly visible. Small clouds are visible both over land and ocean, as well as small-scale waves structures in the cloud deck east of Maui. In this near-IR image, even golf courses and resort developments can be seen along the Hawaiian coastline. The shear zone near the north tip of the island of Hawaii is noticeable as a small, but sharp, discontinuity in the ocean color, with a similar shear zone north of Kahoolawe. Figure 18 presents almost the entire 185 km by 170 km Landsat scene. Figure 19 shows an almost simultaneous DMSP visible image, taken at 2015 on 4 August 1990, two minutes before the Landsat image was collected. The larger area of coverage in the DMSP image gives a better overall view of the cloud patterns upwind and downwind of the islands. While the smallest-scale clouds cannot be seen as clearly in the DMSP image as in the MSS image, the overall cloud patterns are quite well represented. A few thin cirrus clouds are visible in the lower left-hand corner of the Landsat image. These clouds are not well resolved in the DMSP image but contribute to the seemingly anomalous patterns of light and dark that are visible in the sunglint affected areas in the lee of the islands. In this case, the shadows of the thin clouds are often easier to see than the direct reflections from the clouds themselves. Some of the patterns, for example, along the shear zone at the lee of the Kohala Peninsula and just upwind of Lanai, are clearly due to differences in the reflected sunlight, as modulated by differences in sea state.

On 19 July 1990, an MSS image was collected on a much cloudier day. Figure 20 shows a detail of the MSS image, concentrating on the northwest coast of Hawaii. In this case, the shear line at the north end of the island is quite clear. The cloud is quite bright and has saturated the MSS detector with an associated loss of detailed cloud structure information. Wind barbs, corresponding to the simultaneous recorded wind speed and direction from 12 of the automatic weather stations installed as part of HaRP, are shown as an overlay to the satellite imagery. At the north end of the island, the winds reflect the northeasterly trades. In the lee of the island, the onshore flow is reversed

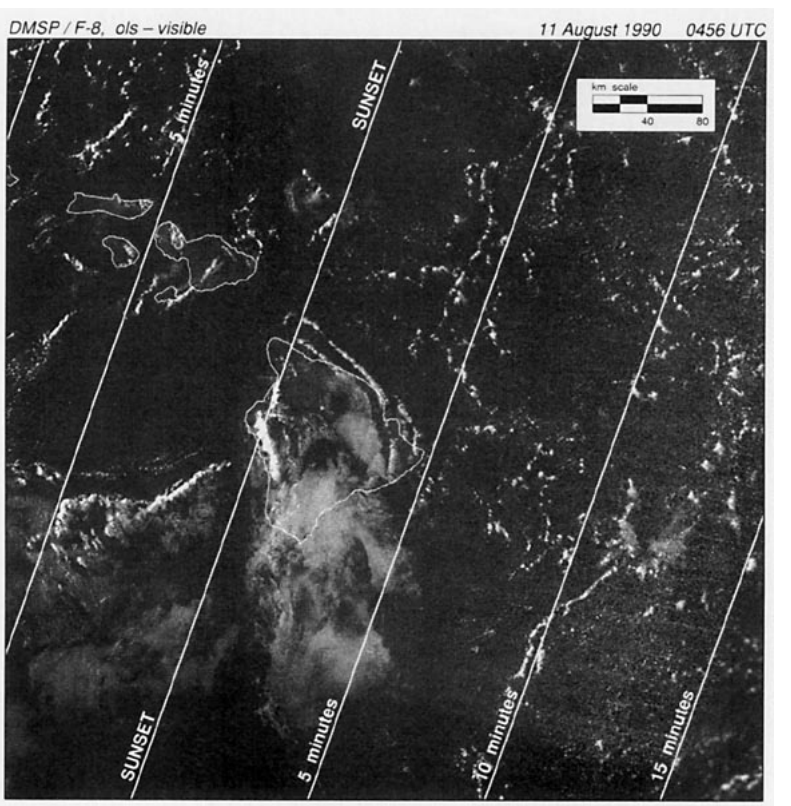

FIG. 16. An OLS visible image at sunset on 10 August 1990 (local time). The overlays indicate the local time before or after sunset across the image.

[3]Cover illustration is a simultaneous multispectral TM image.

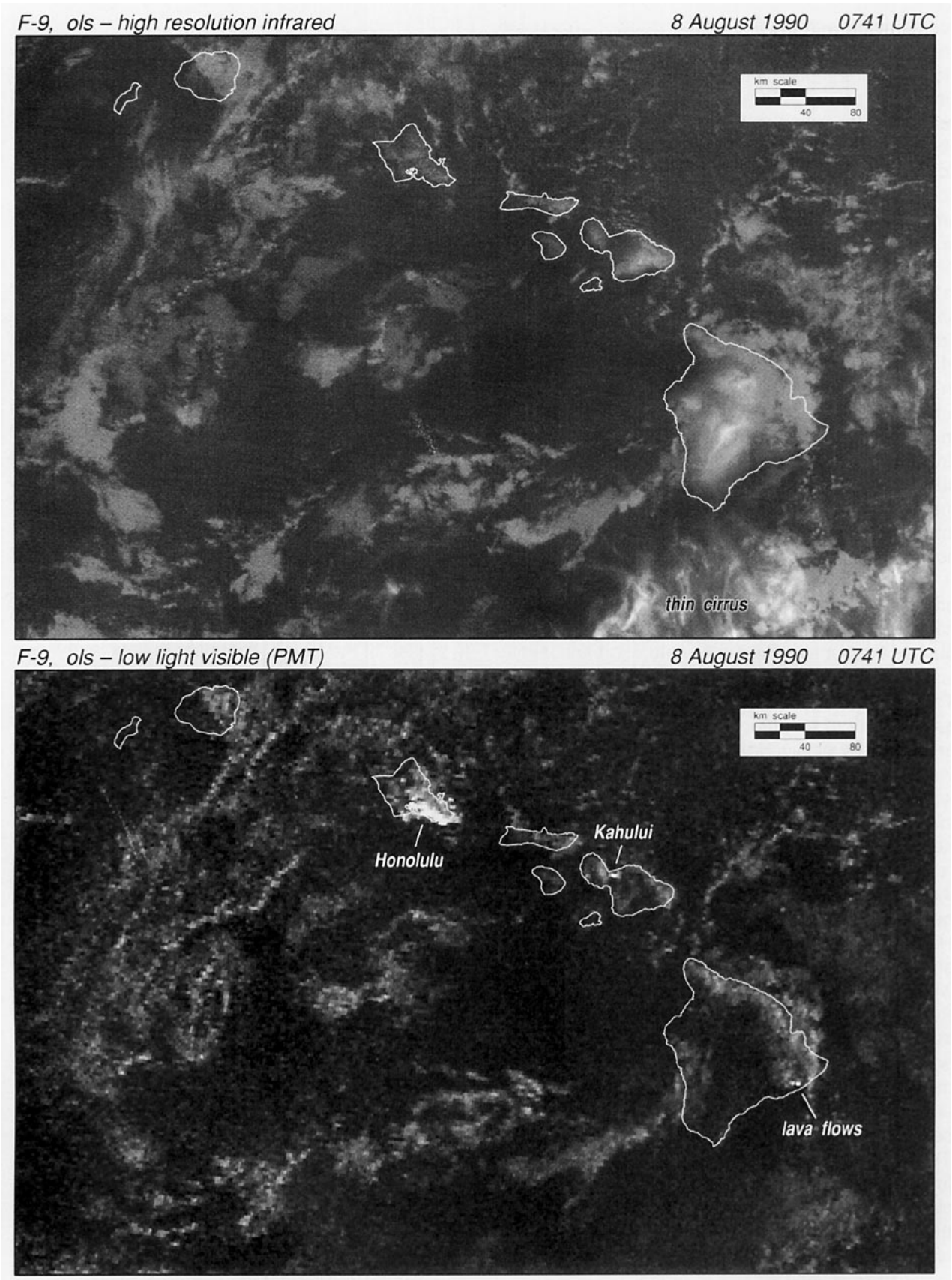

FIG. 17. Nighttime OLS imagery. The top panel shows the high-resolution (550 m at nadir) IR imagery, while the bottom panel shows the simultaneous low-light PMT visible image. Both images were obtained from the DMSP *F-9* satellite at 0741 UTC 8 August 1990.

and relatively weak. Wave structures at a variety of wavelengths and orientations are visible in the middle of the image, near the Waimea "gap" between Mauna Kea and the Kohala Peninsula to the north (see Fig. 25 for elevation contours).

d. SPOT environmental satellites

The SPOT (Satellite Pour l'Observation de la Terre) satellites produce the highest-resolution images that are generally available as digital datasets. The SPOT program is under the direction of the Centre National d'Etudes Spatiales (CNES) in Paris, with imagery distributed by a commercial company, SPOT IMAGE. The first SPOT satellite was launched in February 1986. The current operational satellite in this series is *SPOT-2*.[4] SPOT satellites are positioned in a circular sun-synchronous orbit at an nominal altitude of 830 km, with an orbital period of 101.4 min and orbital inclination of 98.7°. Their equatorial crossing times

[4]The onboard tape recorders have failed on *SPOT-1*, but it is still capable of direct transmission of image data within range of SPOT receiving stations. *SPOT-3* was successfully launched on 25 September.

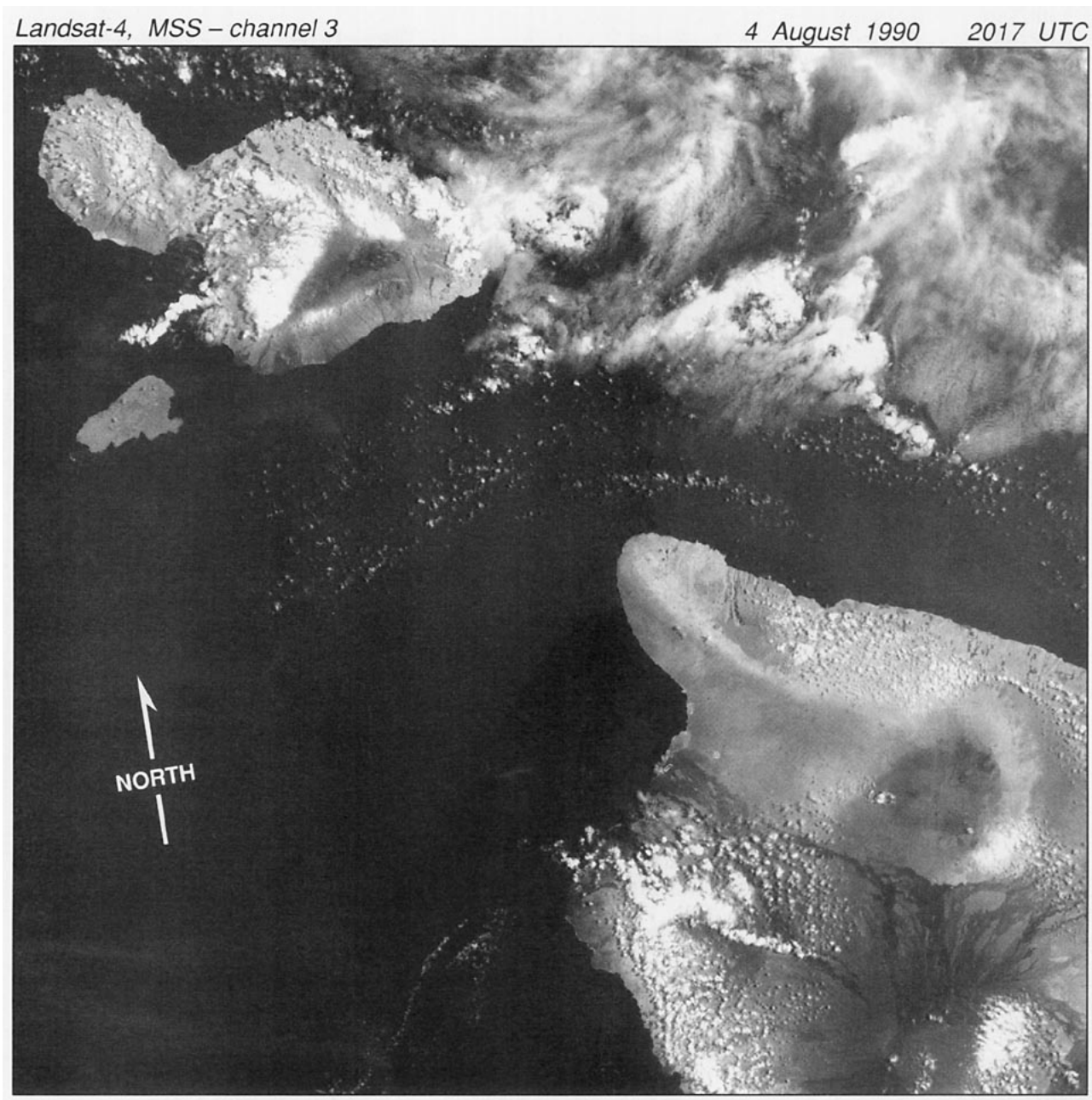

FIG. 18. Landsat MSS image (channel 3, near IR) of Hawaii, Maui, and Kahoolawe obtained on 4 August 1990 at 2017 UTC.

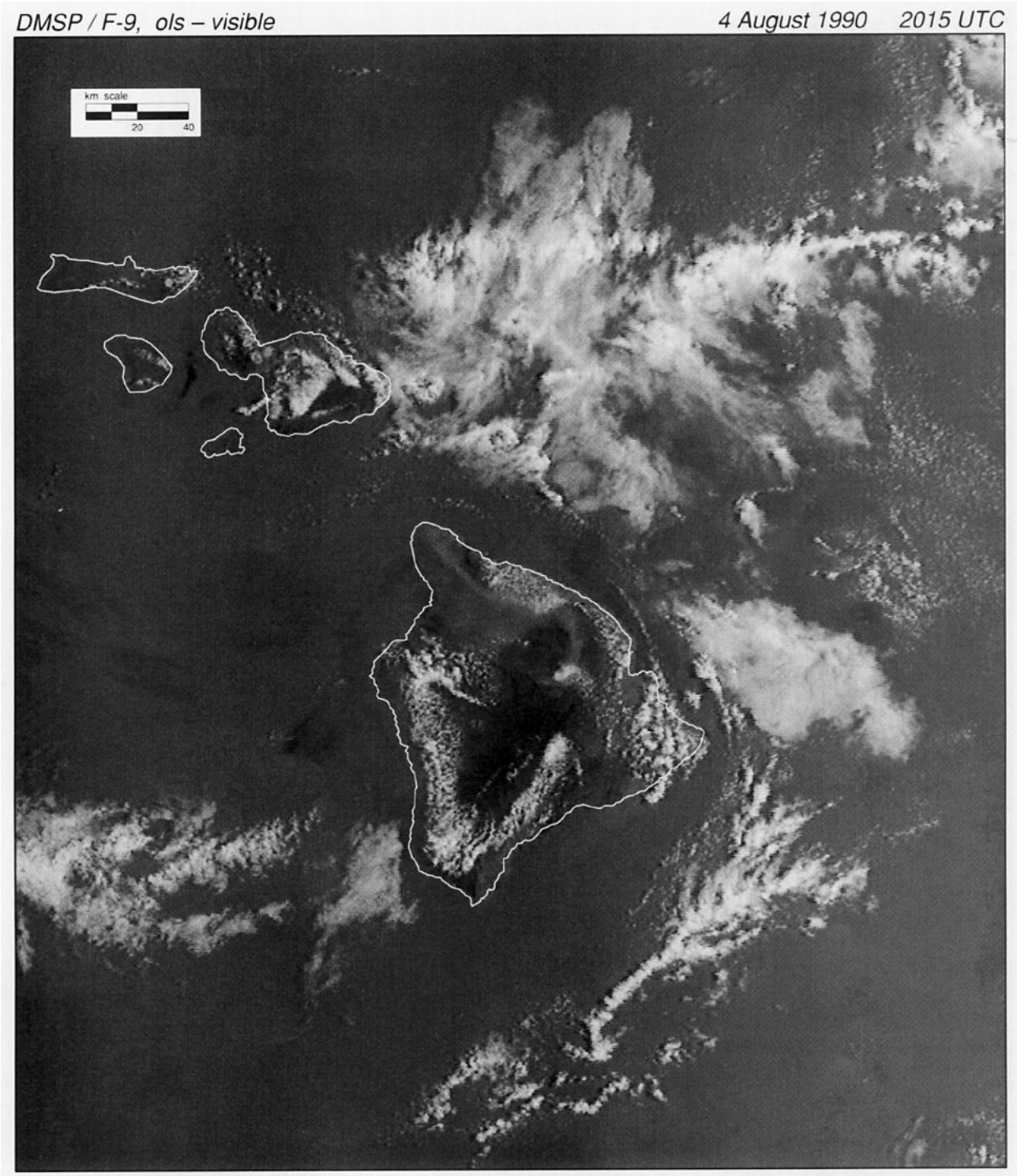

FIG. 19. DMSP visible image from 4 August 1990 at 2015 UTC.

(descending node) are at 1030 LST, with a full orbital repeat cycle taking 26 days (Center National d'Etudes Spatiales 1988a,b; World Meteorological Organization 1989; Massom 1991).

SPOT imagery is obtained by two identical HRV (Haute Resolution dans le Visible) instruments on each satellite that can take data in a multispectral mode involving three spectral bands all in or near the visible spectrum (see Fig. 1), a separate higher-resolution panchromatic mode, or in both modes

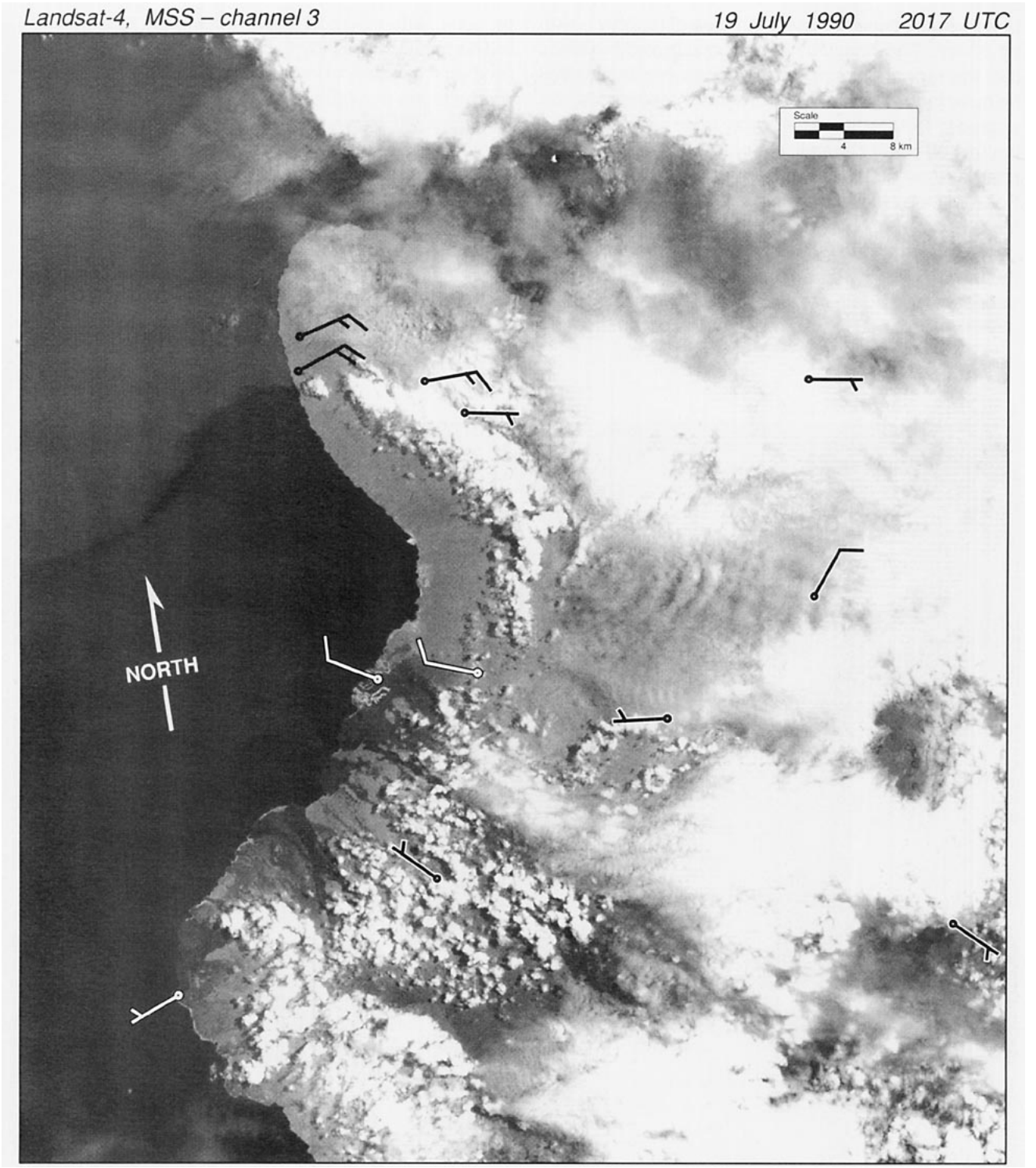

FIG. 20. Landsat MSS image (channel 3, near IR) covering the north end of the island of Hawaii obtained on 19 July 1990 at 2017 UTC. Wind barbs from portable automated mesonet (PAM) stations on the island are superimposed on the image.

simultaneously. The actual sensor elements are a linear array of charge-coupled devices (CCD) aligned in a cross-track or "push broom" configuration. An array of 6000 CCD detectors is used for panchromatic imagery, while 3000 CCD detectors are used for each channel of multispectral data. Panchromatic data have a nominal resolution of 10 m and are quantized to 6-bit accuracy. Multispectral data have a resolution of 20 m and are quantized to 8-bit accuracy. Images, either multispectral or panchromatic, are distributed

as separate scenes covering an area of roughly 60 km by 60 km. The relatively narrow swath width means that the repeat time between successive passes will be quite long. The HRV instruments, however, can be angled to look as far as 27° away from nadir. Employing this off-nadir capability, a specified earth location can be revisited at least once every four or five days. For nadir viewing, simultaneous imagery can be obtained from both HRV instruments, giving a "twin-pair" image 117 km wide, with a 3-km region of overlap in the middle. The HRV instruments have three different user selectable gain settings. Digital images are usually preprocessed for radiometric and geometric corrections, with off-nadir views resampled to maintain the nominal 10- or 20-m resolution. As with the Landsat products, a variety of levels of processing and specific products are available.

Figure 21 shows a full 60 km by 60 km SPOT panchromatic scene, taken on 10 August 1990 at 2118 UTC and centered along the northwest coast of the island of Hawaii. For this image, the HRV instrument was looking toward the east, putting it in position to see sunglint patterns in the sea surface. The sunglint gives a dramatic contrast between the relatively smooth water in the lee of the island and the rougher water of the Alenuihaha Channel, with the shear zone sharply

FIG. 21. SPOT image of the northwest coast of the island of Hawaii. The smooth water in the lee of the island is highlighted by sunglint, showing the location and structure of the shear zone at the north end of the island.

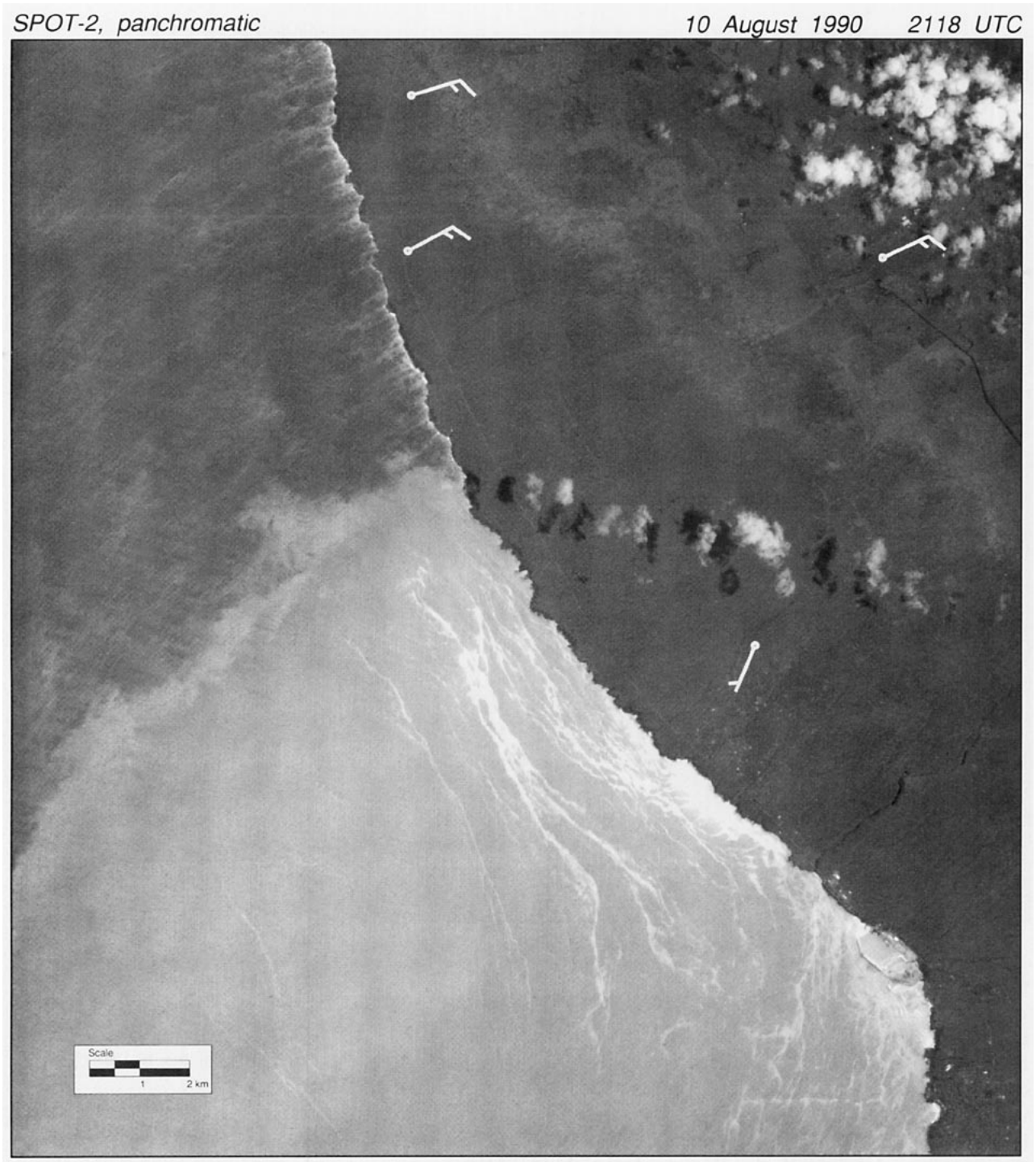

FIG. 22. An enlargement of the coastal section of Fig. 21. Wind barbs from four PAM stations highlight the convergence line that has produced a line of small convective clouds.

delineated. Although this is a relatively cloud-free image, a few very small clouds are visible. Figure 22 shows an enlargement of a portion of the image along the coastline. This detail captures the intersection of the shear zone with the island, extending as far south as Kawaihae Harbor and the Mauna Kea Beach Hotel, located at the curved beach at the extreme bottom of the picture. The irregular bright streaks near the shore line are associated with shoaling internal waves, which produce convergences and highly reflective slicks along their troughs. Looking closely at the jetty at Kawaihae Harbor, it is also possible to see surface waves refracted by bottom topography or reflected by the jetty itself. Over the island, wind barbs from four of

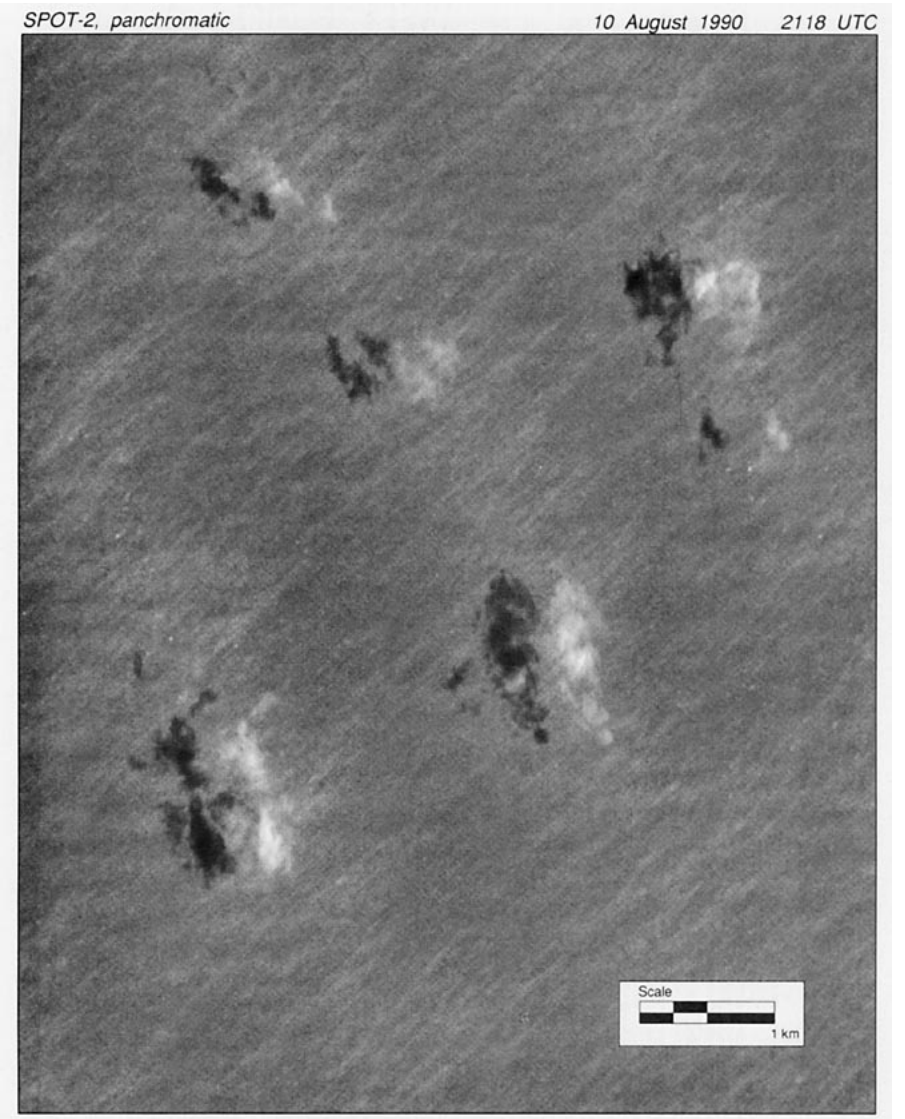

FIG. 23. Enlargement of a section of Fig. 21 over the ocean, showing atmospheric and oceanic waves, as well as small clouds.

the HaRP automatic weather stations have been added to the image. These wind reports document the convergence line associated with the interaction of the weak onshore flow with the northeasterly winds moving over the north end of the peninsula, which produces a line of small clouds. Based on the cloud shadows, these clouds have formed at a height of roughly 1 km above ground. The clouds in the upper right portion of the picture are along the crest of the ridge line and are much closer to the ground. Similar cloud lines can be seen in the same location in many of the other images collected during the project (see Figs. 10, 14, and 20).

Figure 23 is another enlargement of a portion of Fig. 21, this time focusing on the small clouds over the ocean near the upper left corner of Fig. 21. These clouds are associated with what appears to be gravity waves in the trade wind layer of the lower atmosphere. While the clouds are phase locked to the wave crests, the wave structure itself can also be seen in the cloud-free air, presumably through modification of the optical thickness of the marine aerosols by the lifting and sinking motions caused by the waves. Analysis of the cloud shadows indicated that these small clouds are about 750 m above the ocean surface. In the same figure, white streaks aligned with the northeast trade winds correspond to areas of intensified whitecapping. There is also a nearly monochromatic swell, with crests orientated east–west and a wavelength of about 250 m, and smaller wind-driven wave crests perpendicular to the northeast winds at the surface with wavelengths of 30–40 m.

4. Future developments

Both GOES and Landsat are scheduled for significant improvements in their high-resolution imaging capabilities in their next generation spacecraft. In each case, the new spacecraft should be ready for launch in late 1993 or early 1994.[5] The SPOT, DMSP, and NOAA programs are also planning enhancements in their future satellites, but the changes are somewhat farther off.

The new series of GOES satellites (GOES-I through GOES-M) are anticipated to have a number of improvements over the current generation of geostationary satellites. These satellites will have a three-axis stabilization system, like INSAT, instead of the current spin stabilization. This means that the sensors will be able to point at the earth continuously. At present, the spinning sensors only point toward the earth about 5% of the time. Sounding and imaging requirements will be fulfilled by separate instruments. The imager will be

[5] *Lansat 6* was launched on 5 October but failed to reach its intended orbit.

a five-channel scanning radiometer, with one visible channel at 1-km resolution, and four IR channels—three at 4-km resolution and one at 8-km resolution (Rao et al. 1990). All five channels will have 10-bit quantization. While the resolution of the visible channel is not being improved, the additional data bits should improve the quality of the image. Although the basic imaging rate, one full disk scan every 30 min, will be retained, there will be a greater variety of rapid scan modes possible without interfering with the collection of dwell soundings. Unlike the current generation of spin scan radiometers, the new imaging instrument will be able to select its angular scanning limits in both directions. This will permit a more precise placement of a rapid scan window with a faster scan of the area of choice. Like the DMSP's OLS and the Landsat TM instruments, data will be collected in both scan directions.

Unlike *Landsat-4* and *Landsat-5*, *Landsat-6* will not have an MSS imager. The TM, however, will be enhanced with an additional high-resolution panchromatic band that will produce 15-m resolution data over the full 170 km by 185 km scene. A two-level selectable gain setting will be available both for the multispectral and panchromatic modes. In the multispectral mode, the relative gain setting between channels will be modified in the enhanced thematic mapper. At the low gain setting, the mid-IR channels (channels 5 and 7) will have a significantly lower gain than currently available, with a resultant improvement in viewing bright areas, such as clouds, that saturate the current instrument. At the high gain setting, the first four TM channels (visible and near IR) will be more sensitive than the current instrument, permitting improved discrimination in low reflectance areas. This later capability should be advantageous for a number of oceanographic applications.

The next two NOAA polar orbiters to be launched will carry the five-channel AVHRR imaging instrument.[6] The next anticipated upgrade to the AVHRR will not take place until the launch of NOAA-K, scheduled for 1996. Starting with this satellite, the AVHRR instrument will add a sixth channel (1.58–1.64 μm). The second channel will be narrowed a bit to 0.82–0.87 μm. For consistency with the current systems, however, only five channels of data will be transmitted at any one time. At night, the new channel will not be used. During daylight, the existing 3.5–3.7-μm channel will be replaced by the new shorter wavelength channel. This change is anticipated to improve the operational discrimination between cloud and snow cover during daylight hours (Massom 1991). In addition, channels 1 and 2 will have a split gain capability, effectively increasing their digitization to 11-bit accuracy (Needham 1992).

5. Discussion

As evidenced by the preceding discussions and examples, there is an impressive array of satellite imaging devices that can be used for meteorological studies. Each of the systems have its own advantages and disadvantages. Evaluation of the usefulness of any given instrument to a specific problem requires examining the trade off in terms of resolution, angle of view, spectral sensitivity, area of coverage, and repeat frequency. Satellite imagery, however, is most valuable if used in conjunction with data from other sensors, such as surface weather stations, soundings, radars, or in situ measurements of air motion and state parameters from an instrumented aircraft.

Satellite imagery . . . is most valuable if used in conjunction with data from other sensors, such as surface weather stations, soundings, radars, or in situ measurements of air motion and state parameters from an instrumented aircraft.

Figure 24 shows a detail of a DMSP visible image, with a simultaneous overlay of meteorological radar data, showing which clouds have developed areas of precipitation (highlighted in red). The colored areas correspond to equivalent reflectivity factors greater than 20 dB*Z*. The fan-shaped area scanned by the radar is outlined in black, as is the corresponding area scanned by the second Doppler radar, CP-4. Data were recorded to a range of 75 km, but the main dual-Doppler analysis area is restricted to an area relatively near the coast. Even though the precipitating cells are quite small, they can produce precipitation rates in excess of 100 mm h^{-1}. This particular line of cells was one of the largest and best defined rainbands observed during HaRP.

Figure 25 (upper panel) shows an aircraft flight track (black line) and wind vectors (in white) as an overlay on a satellite image that was collected during the flight segment shown. The longer wind vectors, over Alenuihaha Channel, correspond to wind speeds of 10–12 m s^{-1}. The shear zone is sharply defined, with 1–2 m s^{-1} winds flowing back toward the island. As was

[6] *NOAA-13* was successfully launched on 9 August but subsequently lost all power on 21 August.

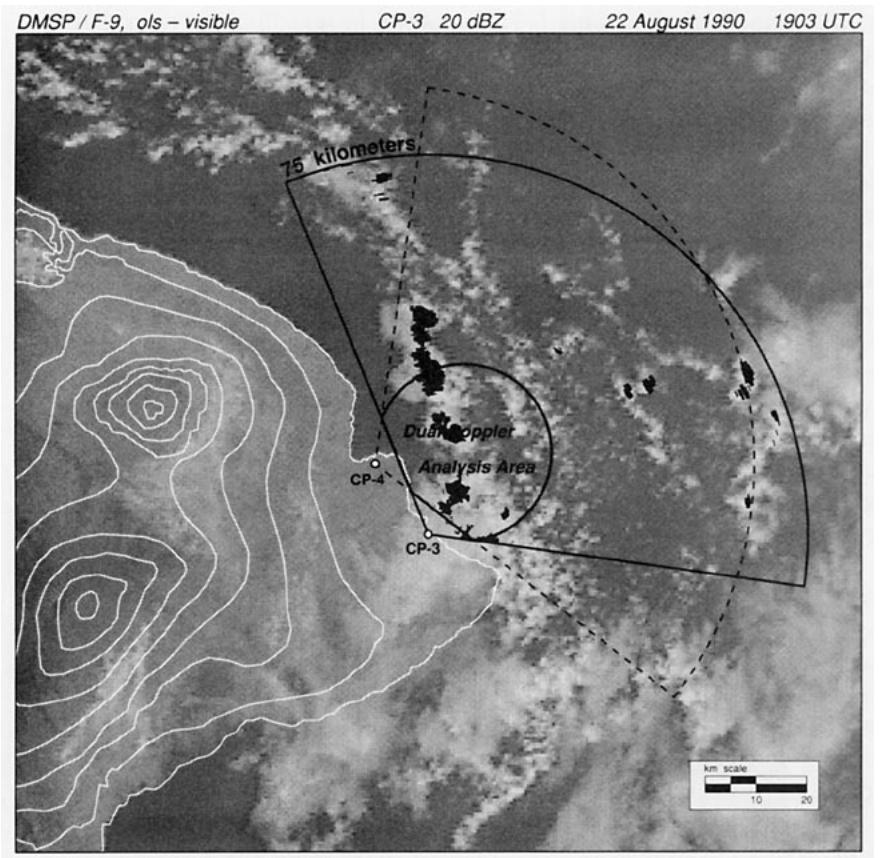

FIG. 24. Weather radar data from the NCAR CP-3 research radar superimposed on a detail of a DMSP satellite image from 22 August 1990 at 1903 UTC. Elevation contours are drawn over the island, with a height interval of 500 m.

done in Fig. 24, the local island topography is indicated by contour lines with a height interval of 500 m. The two major volcanoes on Hawaii are Mauna Kea and Mauna Loa, both rising over 4 km above sea level. On Maui, Haleakala reaches a height of 3 km. Although the sea surface is relatively featureless in this particular image of the shear zone, the earlier *NOAA-10* pass showed considerable structure in the shear zones and island wakes (bottom panel). Somewhat surprisingly, the shear zones in the lee of Oahu and Hawaii are quite straight, while similar zones in the lee of Molokai and Maui show relatively large-scale oscillations. Although the shear zone near the northeast coast of Hawaii is partially obscured by cirrus, the portions of it that are visible are in good agreement with the flight measurements taken an hour later.

Where available, geostationary imagery has usually been the dataset of choice for mesoscale studies. The visible images have remarkably high resolution for a satellite in geostationary orbit, and most importantly, GOES data can give a consistent set of sequential images at a 30-min interval throughout daylight hours. On occasion, imagery is obtained even more frequently. In areas not covered by GOES, the combination of NOAA and DMSP satellites in low earth orbit can give quite good coverage. If possible, it is desirable to collect NOAA data from an HRPT receiving station, since that permits acquisition of direct broadcast data from all functioning NOAA satellites, not just the two satellites defined as "operational." Even if GOES data are available, imagery from polar-orbiting satellites can be a valuable addition to a study, giving data with a different viewing angle and sensor characteristics.

The DMSP satellites are a potentially valuable resource but, until recently, have seen limited use outside of the U.S. Department of Defense. The growing availability of digital DMSP datasets is likely to result in increased use of the high-resolution OLS imagery. The high resolution of the data, and the unique ability to preserve the effective resolution of the image across the entire swath width, makes this dataset particularly well suited for small-scale meteorological studies. Even though a number of recent projects have been successful at acquiring digital DMSP imagery (through the cooperation of the U.S. Department of Defense), the continuing encryption of the real-time direct broadcast data will continue to limit its utilization for nonmilitary operational applications.

Very high resolution imagery from SPOT and Landsat are in a completely different class. The resolution cannot be even approached by the standard meteorological satellites. A Landsat or SPOT image can give a detailed

FIG. 25 (see facing page). Morning satellite images from 6 August 1990 during an aircraft flight to investigate the northern shear zone. The bottom panel shows a *NOAA-10* image from 1827 UTC that documents the larger-scale structure of the shear zone, made visible by sunglint. The top panel shows a subsequent DMSP image, taken at 1934 UTC. The aircraft flight track, wind vectors, and elevation contours (500-m height increment) on the surrounding islands are superimposed on the image.

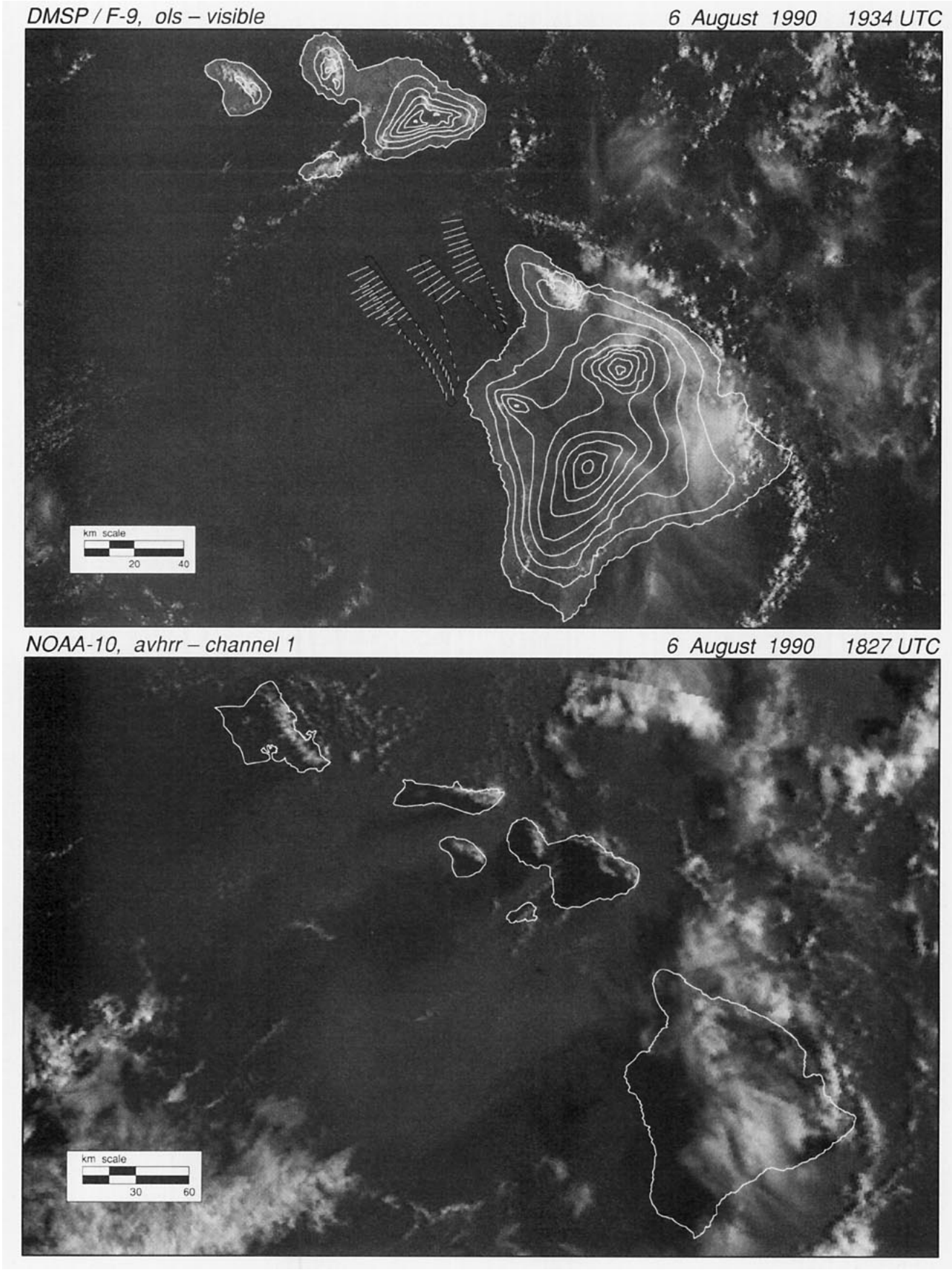
DMSP / F-9, ols – visible
6 August 1990 1934 UTC
km scale
20 40
NOAA-10, avhrr – channel 1
6 August 1990 1827 UTC
km scale
30 60

view that could otherwise only be achieved by high-altitude planes taking aerial photographs. The tradeoffs are the lack of diurnal coverage, long repeat time (days) between images, and no capability for acquiring and displaying images in real time. For research applications, however, the data can be quite valuable and these high-resolution images have probably not been used as much as they should. The lack of daily coverage is particularly troublesome for most meteorological studies. In the case of SPOT, however, the off-nadir viewing capability does significantly increase the availability of coverage. For many applications, however, the area covered may be just too small. In that sense, the Landsat field of view (185 by 170 km) may often be better. Unfortunately, the Landsat satellites do not have "off-nadir" viewing capabilities, so increased coverage only comes through use of more than one satellite (two are now operational). *Landsat-6* will combine high-resolution panchromatic imagery and relatively wide viewing swath.

At one time, satellite data processing was the preserve of large data centers and mainframe computers. With the increasing availability of powerful workstations, it is now possible to process satellite data effectively in a wide variety of environments. Merely displaying images, however, is only one aspect of a modern satellite data system. It is also essential to have orbital information for the satellites of interest in order to calculate viewing angles relative to the surface and relative to solar reflections. Modern software and data navigation techniques can be used to remap satellite images to standard data planes or map projections, removing the distortion that was so familiar in the earliest imagery. This greatly facilitates the merging of different datasets and should be done routinely.

The critical issue, both for research and operational applications, is data access. Through increased use of direct receiving stations and high-speed data networks, satellite data should become increasingly available to a variety of users. With increased availability, the use of satellite data for meteorological applications will grow and diversify.

Acknowledgments. During HaRP, digital DMSP and NOAA HRPT data were archived using a TeraScan workstation, operated by SeaSpace Corporation under contract with the National Center for Atmospheric Research (NCAR). This workstation was installed at Hickam AFB, Honolulu, with the cooperation of the U.S. Air Force First Weather Wing, Col. T. K. Klein, Commander. HRPT data were also recorded at the University of Hawaii, Honolulu, using a separate TeraScan acquisition system supported by National Science Foundation Grant OCE-8918604. Acquisition of SPOT imagery was funded by the National Aeronautics and Space Administration Contract SIR-C-093 to the University of Hawaii. Satellite data were processed using TeraScan software at the University of Hawaii, SeaSpace Corporation, and NCAR. PostScript image files were printed on a Linotronic 300 Phototypesetter by Image Systems, Boulder, Colorado.

We appreciate receiving comments and suggestions from Jim Wilson and Chris Ennis, NCAR; Mike Van Woert,[7] SeaSpace Corporation; Tom Lee, Naval Research Laboratory, Monterey, California; Steve Smith, Cooperative Institute for Research in the Atmosphere (CIRA), Colorado State University, Fort Collins; and Tina Cary, EOSAT.

Landsat imagery is reproduced by permission of the Earth Observation Satellite Company (EOSAT), Lanham, Maryland. SPOT imagery is copyrighted by the Centre National d'Etudes Spatiales (CNES) and is reproduced by permission of SPOT Image Corporation, Reston, Virginia.

References

Arking, A., and J. D. Childs, 1985: Retrieval of cloud cover parameters from multispectral satellite images. *J. Climate Appl. Meteor.*, **24,** 322–333.

Bernstein, R. L., 1982: Sea surface temperature estimation using the *NOAA-6* Advanced Very High Resolution Radiometer. *J. Geophys. Res.*, **87,** 9455–9465.

Breaker, L. C., 1990: Estimating and removing sensor-induced correlation from Advanced Very High Resolution Radiometer satellite data. *J. Geophys. Res.*, **95,** 9701–9711.

Clark, J. D., Ed., 1983: *The Goes User's Guide.* U.S. Department of Commerce (NOAA/NESDIS), 162 pp.

Cloakley, J. A., R. L. Bernstein, and P. A. Durkee, 1987: Effect of ship-track effluents on cloud reflectivity. *Science,* **237,** 1020–1022.

Centre National d'Etudes Spatiales, 1988a: *SPOT User's Handbook. Volume 1: Reference Manual.* SPOT Image Corp., 305 pp.

——, 1988b: *SPOT User's Handbook. Volume 2: SPOT Handbook.* SPOT Image Corp., 452 pp.

Cram, R., and K. Hanson, 1974: The detection by ERTS-1 of wind-induced ocean surface features in the lee of the Antilles Islands. *J. Phys. Oceanogr.,* **4,** 594–600.

de Waard, J., W. P. Menzel, and J. Schmetz, 1992: Atlantic data coverage by *Meteosat-3. Bull. Amer. Meteor. Soc.,* **73,** 977–983.

——, 1993: Extended Atlantic weather coverage provided by *Meteosat-3. European Space Agency Bull.*, **74,** 20–27.

Dousset, B., P. Flament, and R. Bernstein, 1993: Los Angeles fires seen from space. *Transactions, American Geophysical Union (EOS),* **74**(33), 37–38.

Eden, H. F., B. P. Elero, and J. N. Perkins, 1993: Nimbus satellites: Setting the stage for Mission to Planet Earth. *Transactions, American Geophysical Union (EOS),* **74,** 281, 285.

Engelstad, M., S. K. Sengupta, T. Lee, and R. M. Welch, 1992: Automated detection of jet contrails using the AVHRR split window. *Int. J. Remote Sensing,* **13,** 1391–1412.

d'Entremont, R. P., 1986: Low- and midlevel cloud analysis using nighttime multispectral imagery. *J. Climate Appl. Meteor.,* **25,** 1853–1869.

Fermelia, L. R., 1982: The design and development of GOES. *Meteorological Satellites—Past, Present, and Future.* NASA Conference Publication 2227, 35–42.

Fett, R. W., and K. M. Rabe, 1976: Island barrier effects on sea state as revealed by a numerical wave model and DMSP satellite data. *J. Phys. Oceanogr.,* **6,** 324–334.

——, and R. G. Isaacs, 1979: Concerning the causes of "anomalous gray shades" in DMSP visible imagery. *J. Appl. Meteor.,* **18,** 1340–1351.

[7]Current affiliation: NASA Headquarters, Washington, D.C.

——, and S. D. Burk, 1981: Island barrier effects as observed by satellite and instrumented aircraft, and simulated by a numerical model. *Mon. Wea. Rev.*, **109,** 1527–1541.

——, W. A. Bohan, J. J. Bates, and S. L. Tipton, 1983: Navy tactical applications guide: Operational environmental satellites. Tech. Rep. 83-02, Naval Environmental Prediction Research Facility, 70 pp.

Flannigan, M. D., and T. H. Vander Haar, 1986: Forest fire monitoring using NOAA satellite AVHRR. *Canadian J. Forestry Research,* **16,** 975–982.

Foster, J. L., and D. K. Hall, 1991: Observations of snow and ice features during the polar winter using moonlight as a source of illumination. *Remote Sens. Environ.*, **37,** 77–88.

Fujita, T. T., D. L. Bradbury, C. Merrino, and L. Hull, 1968: A study of mesoscale cloud motions computed from ATS-1 and terrestrial photographs. Satellite and Mesometeorology Research Project Paper No. 71, University of Chicago, 25 pp.

Gibson, J., Ed., 1984: *GOES Data User's Guide.* U.S. Department of Commerce (NOAA/NESDIS), 142 pp.

Goody, R. M., 1964: *Atmospheric Radiation: Part I. Theoretical Basis.* Clarendon Press, 436 pp.

Goyette, J. A., W. D. Klein, and A. L. Adams, 1990: The defense meteorological satellite program review. Preprints, *Fifth Conf. on Satellite Meteor. and Ocean.*, London, Amer. Meteor. Soc., 455–458.

Haas, I. S., and R. Shapiro, 1982: The Nimbus satellite system—Remote sensing R&D platform of the 70's. *Meteorological Satellites—Past, Present, and Future.* NASA Conference Publication 2227, 17–29.

Hill, J., 1991: *Weather from Above: America's Meteorological Satellites.* Smithsonian Institution Press, 89 pp.

Hollinger, J. P., J. L. Pierce, and G. A. Poe, 1990: SSM/I instrument evaluation. *IEEE Trans. Geoscience and Remote Sensing,* **28,** 781–790.

Isaacs, R. G., and J. C. Barnes, 1987: Intercomparison of cloud imagery from the DMSP OLS, NOAA AVHRR, GOES VISSR, and Landsat MSS. *J. Atmos. Ocean. Tech.*, **4,** 647–667.

Khattak, S., R. A. Vaughan, and A. P. Cracknell, 1991: Sunglint and its observation in AVHRR data. *Remote Sens. Environ.*, **37,** 101–116.

Kidwell, K. B., Ed., 1991: *NOAA Polar Orbiter Data Users Guide.* U.S. Department of Commerce (NOAA/NESDIS), 294 pp.

Klein, W. D., G. A. Mandt, and J. Gagliardo, 1992: Defense meteorological satellite program. Preprints, *Sixth Conf. on Satellite Meteor. and Ocean.* Atlanta, Amer. Meteor. Soc., 450–452.

Langland, R. H., P. M. Tag, and R. W. Fett, 1987: Numerical simulation of a satellite-observed calm zone in Monterey Bay, California. *Wea. Forecasting,* **2,** 261–268.

Lee, T. F., 1989: Jet contrail identification using the AVHRR split window. *J. Appl. Meteor.*, **28,** 993–995.

——, and P. M. Tag, 1990: Improved detection of hotspots using the AVHRR 3.7 μm channel. *Bull. Amer. Meteor. Soc.,* **71,** 1722–1730.

Lillesand, T. M., and R. W. Kiefer, 1987: *Remote Sensing and Image Interpretation.* John Wiley and Sons, 721 pp.

Lyons, W. A., and T. Fujita, 1968: Mesoscale motions in oceanic stratus as revealed by satellite data. *Mon. Wea. Rev.*, **96,** 304–314.

Mason, B., and J. Schmetz, 1992: Meteorological satellites. *Int. J. Remote Sensing,* **13,** 1153–1172.

Massom, R., 1991: *Satellite Remote Sensing of Polar Regions: Applications, Limitations and Data Availability.* Belhaven Press, 307 pp.

McClain, E. P., and A. E. Strong, 1969: On anomalous dark patches in satellite-viewed sunglint areas. *Mon. Wea. Rev.*, **97,** 875–884.

——, W. G. Pichel, and C. C. Walton, 1985: Comparative performance of AVHRR-based multichannel sea surface temperatures. *J. Geophys. Res.*, **90,** 11 587–11 601.

Meyer, W. D., 1973: Data acquisition and processing program: A meteorological data source. *Bull. Amer. Meteor. Soc.*, **54,** 1251–1254.

Needham, B. H., 1976: Observation of wind-induced sea surface feature off Pulu Bawean, Java, from *Landsat-1. Bull. Amer. Meteor. Soc.*, **57,** 444–448.

——, 1992: Advanced instrumentation and services from NOAA operational polar satellites. Preprints, *Sixth Conf. on Satellite Meteor. and Ocean.*, Atlanta, Amer. Meteor. Soc., 442–445.

Price, J. C., 1991: Timing of NOAA afternoon passes. *Int. J. Remote Sensing,* **12,** 193–198.

Purdom, J. F. W., 1976: Some uses of high-resolution GOES imagery in the mesoscale forecasting of convection and its behavior. *Mon. Wea. Rev.*, **104,** 1474–1483.

Rao, P. K., S. J. Holmes, R. J. Anderson, J. S. Winston, and P. E. Lehr, 1990: *Weather Satellites: Systems, Data, and Environmental Applications.* Amer. Meteor. Soc., 503 pp.

Rivers, J. W., and C. P. Arnold, 1982: Defense Meteorological Satellite Program (DMSP). *Meteorological Satellites—Past, Present, and Future.* NASA Conference Publication 2227, 31–34.

Robinson, I. S., N. C. Wells, and H. Charnock, 1984: The sea surface thermal boundary layer and its relevance to the measurement of sea surface temperature by airborne and spaceborne radiometer. *Int. J. Remote Sensing,* **5,** 19–45.

Saunders, R. W., and K. T. Kriebel, 1988: An improved method for detecting clear sky and cloudy radiances from AVHRR data. *Int. J. Remote Sensing,* **9,** 123–150.

Schnapf, A., 1982: The development of the TIROS global environmental satellite system. *Meteorological Satellites—Past, Present, and Future.* NASA Conference Publication 2227, 7–16.

Scorer, R. S., 1986a: Etna: The eruption of Christmas 1985 as seen by meteorological satellite. *Weather,* **41,** 378–384.

——, 1986b: *Cloud Investigation by Satellite.* Ellis Horwood, 314 pp.

——, 1990: *Satellite as Microscope.* Ellis Horwood, 268 pp.

Shenk, W. E., T. H. Vonder Haar, and W. L. Smith, 1987: An evaluation of observations from satellites for the study and prediction of mesoscale events and cyclone events. *Bull. Amer. Meteor. Soc.*, **68,** 21–35.

Smith, R. B., and V. Grubisic, 1993: Aerial observations of Hawaii's wake. *J. Atmos. Sci.*, **50,** 3728–3750.

Strong, A. E., R. J. DeRycke, and H. G. Stumpf, 1974: Extensive areas of reduced waves leeward of the Lesser Antilles. *Geophys. Res. Lett.*, **1,** 47–49.

Yamanouchi, T., K. Suzuki, and S. Kawaguchi, 1987: Detection of clouds in Antarctica from infrared multispectral data of AVHRR. *J. Meteor. Soc. Japan,* **65,** 949–962.

Van Woert, M. L., R. H. Whritner, D. E. Waliser, D. H. Bromwich, and J. C. Comiso, 1992: ARC: A source of multisensor satellite data for polar science. *Transactions, American Geophysical Union (EOS),* **73**(65), 75–76.

Wald, L., and J. M. Monget, 1983: Remote sensing of the sea-state using the 0.8–1.1 μm spectral band. *Int. J. Remote Sensing,* **4,** 433–446.

Williams, S. F., K. Caesar, and K. Southwick, 1992: The Convection and Precipitation Electrification Experiment (CaPE): Operations summary and data inventory. National Center for Atmospheric Research, Office of Field Project Support, 425 pp.

World Meteorological Organization, 1989: *Information on Meteorological and Other Environmental Satellites (2d edition).* WMO No. 411, 168 pp.